A Novel Flexible Distributed Pressure Sensing Strip for a Urethral Catheter

A DISSERTATION
SUBMITTED TO THE FACULTY OF THE GRADUATE SCHOOL
OF THE UNIVERSITY OF MINNESOTA
BY

Mahdi Ahmadi

IN PARTIAL FULFILLMENT OF THE REQUIREMENTS
FOR THE DEGREE OF
DOCTOR OF PHILOSOPHY

Adviser: Rajesh Rajamani

June 2017

ACKNOWLEDGMENTS

In this single page I want to thank every teacher that I had in my life, since my first grade till the last. Also I want to thank any person who intentionally or unintentionally taught me and helped me to grow in my scientific life. My dad showed me the first doors to the mysteries of world of science, my mom was the main supporter for me throughout my long journey in education and research, and my sister was my companion in it. I have been so lucky to meet many interesting people with different scientific and cultural backgrounds who shaped my scientific view and reminded me not to forget humanity in my career.

I want to thank Rajesh Rajamani my PhD adviser who helped me and showed me the way of being a professional researcher in our time. My dream of working in the micro and nano scale world, became real through his lab. Also I want to thank Gerald Timm for always bringing support and creative ideas to the project. I want to thank Arthur Erdman for being very persuasive and supportive in the first two years of my PhD. It was my honor to have Rusen Yang and Suhasa Kodandaramaiah in my final examination committee to review my work. I want to thank Serdar Sezen who was a nice friend and also the person who introduced me to micro-fabrication.

I had a great time with my lab mates in room 13 in the basement of mechanical engineering department, from January 2011 to May 2017, in summers and winters. I will miss you Kalpesh, Garrett, Peng, Shan, Gridsada, Song, Ye, Corey, Yan and Ryan.

And thank you Laura for being part of my life and all the support, joy and happiness that you brought to my life.

DEDICATION

To all the animals who have helped us in laboratory experiments for ages.

ABSTRACT

This dissertation develops, designs, fabricates and evaluates an instrumented catheter for instantaneous measurement of distributed urethral pressure profiles. The developed catheter has important clinical applications in urodynamic testing for analyzing the causes of urinary incontinence in patients. A flexible sensor strip is fabricated with an array of nine pressure sensors and integrated electronic pads for an associated sensor IC chip. The flexible sensor strip and associated IC chip are assembled on a 7 Fr Foley catheter for the urology application.

There are two major challenges in the development of the sensor strip. First, a highly sensitive sensor strip that is flexible enough for urethral insertion into a human body is required and second, the sensor should work reliably in a liquid in-vivo environment in the human body. Capacitive force sensors are designed and micro-fabricated using polyimide/PDMS substrates and copper electrodes. To remove the stray influence of urethral tissues which create fringe capacitance that can lead to significant errors, a reference fringe capacitance measurement sensor is incorporated on the strip and the whole sensor area is actively shielded in a Faraday cage made of gold. By supplying the active sensing voltage simultaneously to the deformable electrode of the capacitive sensor and to the Faraday cage, the stray capacitance during in vivo measurements can be largely eliminated. Due to the transparency of the Faraday cage, the top and bottom portions of a capacitive sensor can be accurately aligned and assembled together. Experimental results presented in the thesis show that stray capacitance is reduced by an order of magnitude by the Faraday cage when the sensor is subjected to a full immersion in water.

Since the catheter enables a new type of urological measurement, a process for accurate ex-vivo validation of the catheter is also developed. A sheep bladder and urethra are extracted and used in an ex-vivo set up for validation of the developed instrumented catheter. The bladder-urethra are suspended in a test rig and pressure cuffs placed to apply known static and dynamic pressures around the urethra. An algorithm based on use of reference stray transducers is used to compensate for the remaining portion of stray capacitance. Extensive experimental results verify that the developed compensation method works effectively. Results on pressure variation profiles circumferentially around the urethra and longitudinally along the urethra are presented.

Finally, the developed sensing catheter is tested in vivo in live female sheep to construct real-time urethral pressure profiles. The results are presented and discussed.

TABLE OF CONTENTS

LIST OF FIGURES

Chapter 1

1 INTRODUCTION

The bladder and the urethra are the main parts of the lower urinary tract (Figure 1). If functioning well, they store incoming urine from the upper urinary tract without any leakage or urgency of voiding. In normal micturition (urination), evacuation starts by voluntarily controlling the external urethral sphincter and detrusor. This delicate function can be altered by neurogenic or mechanical failures which if present can lead to urinary incontinence (UI) in patients. UI is "the complaint of any involuntary leakage of urine" [1]. UI is believed to affect at least 13 million people in the United States, 80% of them women [2], [3], [4], [5], [6], [7], [8] and [9].

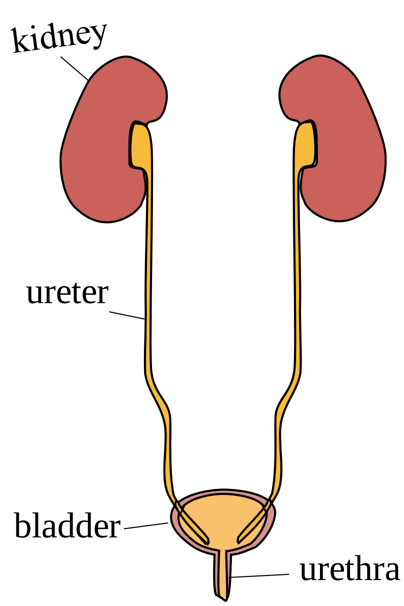

Figure 1: Human urinary system

A standard approach currently used to diagnose and determine the appropriate treatment for patients suffering from UI is urodynamics [10]. Urodynamics studies are used to measure storage and voiding functions of the urinary bladder and the urethra. Urodynamics normally consists of two main phases [11]. First, cystometry to investigate the storage function in the bladder during filling, including the ability to store without leakage during provocative maneuvers such as coughs and stationary jogging. During these tests a thin, flexible catheter is inserted into the bladder through the urethra. The most advanced catheter on the market is a micro-tip catheter with a single pressure sensor at the tip. Current methods for recording distributed urethral closure pressures require pulling the same single microtip pressure sensing catheter through the urethra in order to measure pressure at different locations in the urethra, thereby eliminating the ability to conduct real-time, provocative tests such as coughing, val salva and in-spot jogging. The cost of a single microtip catheter is extremely high (> $2000) and so even the use of these inadequate catheters poses a significant health cost. The second phase is single point pressure-flow measurement in the bladder and then the urethra to examine urine voiding performance and urethral closure pressure. Further ambulatory urodynamic studies with natural filling have also been applied for patients to avoid the unnatural environment of the urodynamic tests [12]. Ambulatory studies have been found useful for confirming overactive detrusor muscle activity in patients for whom conventional urodynamic tests failed to reproduce symptoms [13]. Intravaginal or peri-anal electrode is used to additionally measure the electrical activity of the pelvic floor muscles [14].

1.1 Historical Development of Urethral Pressure Measurement Techniques

The first clinical method to measure urethral pressure (P_{ura}) was introduced in 1960 by Lapides et al. [15]. They measured P_{ura} by measuring fluid pressure in direct contact with urethral walls. In this method, a whistled-tip catheter was inserted into the urethra. At its distal end the catheter was connected to a manometer which was filled with enough water to ensure that water can discharge in the urethra (Figure 1a). Water height would go down in the manometer until pressure from the walls in the urethra was equal to water column pressure. That pressure was recorded as pressure at that specific point in urethra. To measure urethral pressure profile (UPP), the measurement had to be repeated at many points in the urethra. Not only was this laborious and time consuming, it was also not possible to get real time data for provocative actions. In 1967 Brown and Wickham went farther and proposed a new method by defining P_{ura} as the pressure needed for a liquid to slightly open the collapsed urethral walls [16]. In their method, a urethral catheter with side holes was used. A syringe connected to the catheter stands outside the urethra to pump the fluid into the bladder and a pressure transducer is connected to this hydrodynamic system to measure the pressure in the liquid. During the test the inserted catheter is manually drawn through the urethra to measure the pressure at different points and construct the UPP (Figure 2b). In this method, it is important to remove all the bubbles from the tubes carefully. Otherwise the readings will be altered by air compressibility. Like the Lapides's method, the Brown-Wickham method needs tubing and external setups to do the measurement. Moreover, the Brown-

Wickham method cannot create a urethral pressure profile during fast maneuvers like coughing and Valsalva.

The modern solution to measuring urethral pressure is using a cylindrical balloon that is mounted on a catheter [17]. The fluid in the balloon (Figure 2c) that transmits pressure signal to the external pressure transducer could be either water or air [18]. The water filled balloon’s bandwidth is larger than the air charged ones that makes them suitable for pressure measurements in provocative maneuvers [18]. The balloon should be partially charged otherwise the elastic force in the balloon’s membrane makes the pressure change inside the balloon different than real pressure change inside the urethra. In this method, the balloon averages out the pressure in both circumferential and longitudinal directions inside urethra. In case of using water as the medium, the external transducer outside body should be leveled by the catheter tip to avoid error in pressure measurement. The air charged catheters do not need the transducer to be leveled by the catheter tip but their response is slow [18]. Again, to measure the UPP, the catheter should be moved slowly through the urethra and pressure should be recorded by the external setup. There is no possibility to get real time distributed data in the urethra, therefore the study of sudden changes in abdominal pressure like coughing is not possible.

Alternatively, the pressure transducer can be placed on the tip of catheter itself, like fiber-optic catheters with a single pressure sensor at the tip [19]. Their bandwidth is high and good for measuring sudden changes in abdominal pressure. Also, they are free of tubing complexities like levelling and bubble removal from the liquid. These sensors are expensive and not disposable and since the transducer is mounted at the tip of the catheter the pressure measurement is performed between rather than at the urethral walls. So the pressure is different than urethral pressure. Moreover, the catheter still needs to be moved slowly through the urethra to construct the UPP [11].

The development of micro sensors for pressure and force measurement is in general a topic of strong interest and has been pursued recently for a variety of applications [20], [21], [22], [23]. To move beyond currently available techniques, we developed a new inexpensive disposable instrumented Foley catheter with a continuous array of flexible capacitive pressure sensors on it. This sensing strip is placed along 4 cm of the catheter to measure pressure in real time and send the data to a capacitance to digital signal converter chip that is mounted on the catheter. Placing the capacitance to digital converter chip on the sensing strip reduces the signal lines and hence the stray capacitance. A convenient plug-in interface cable eliminates the complexity of tubing and transmitting pressure to an external transducer and also in the case of using water filled catheters it avoids air bubble removal. To obtain adequate sensitivity for measurement of low urethral pressures, capacitive sensors with small micron-sized air-gaps on a flexible substrate are utilized. This sensor strip can be utilized with 7 Fr and larger catheters. The proposed technique provides instantaneous real-time measurement of the distribution of pressure and can be used for urethral measurement during provocative maneuvers, such as coughing, pressing the stomach, or in stationary jogging.

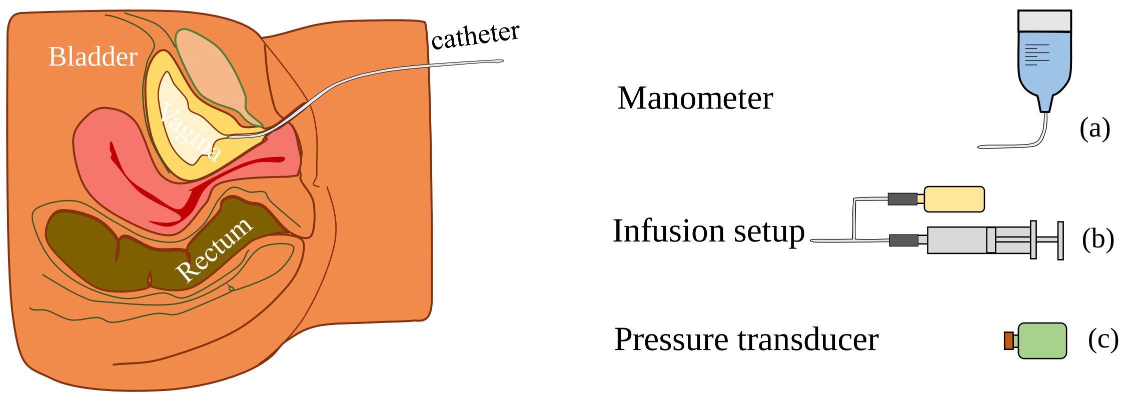

Figure 2: Urodynamics in a female patient: (a) Lapides's method using a manometer, (b) Brown-Wickham method for constructing UPP by constant low volume rate of perfusion and an external transducer, (c) air/water-charged balloon sensor.

1.2 Review of Available Pressure Sensing Technologies

Various force/contact-pressure sensing mechanisms could be explored for urethral pressure measurement [24], [25], [26], [27], [28], [29], [30], [31], [32], [33]. Piezoelectric sensors [34] could not be used for this application, since typical piezoelectric materials do not measure static forces and the pressure distribution to be measured in this application is either static or varying very slowly in time [35]. Piezoresistive sensors [36] could not be used either, since they are susceptible to drift and require either calibration just before the measurement or compensation to be able to measure absolute pressures with accuracy. Given the small size of the catheter, it was therefore decided to use the flexible capacitive sensing mechanism [37], [38], [39], due to its high sensitivity for measuring low and static force/pressure with adequate resolution [40], [41], [42].

1.3 Stray Capacitance- A Significant Challenge

Capacitive pressure sensors are highly sensitive to pressure change and have superior low-drift properties with temperature and humidity, compared to those of piezo-resistive devices. But capacitive sensors suffer from an inherent problem that has been rarely recognized or addressed in literature – They suffer from significant stray capacitance induced by the body during in vivo applications [43], [44]. Hence, in vivo applications of capacitive sensors typically measure dynamic variables, rather than absolute (or static) values [45], [46]. In chapter 4 of this dissertation we address stray capacitance by developing a Faraday cage that encloses the sensor and is utilized electrically during capacitance measurement to shield against fringe fields from the human body. We will show how the Faraday cage can be made transparent to enable assembly of separately fabricated sensor components, and can yet function effectively.

1.4 Thesis Objectives

The objective of this research is to

i- develop a pressure sensing catheter with a capability to measure contact pressure or forces at multiple locations in the urethra.

ii- develop an ex-vivo validation procedure using an extracted sheep bladder and urethra as a platform for urodynamics.

iii- conduct in vivo tests in female sheep.

The developed catheter will provide simultaneous measurement of pressure at multiple locations in the urethra with one static device, instead of the current technique of moving the device to measure pressure at one location at a time. The proposed sensor system relies on an inexpensive disposable sensor strip.

The developed sensing device will be highly flexible for insertion into the urethra and highly compact for inclusion on a 2.6 (mm) diameter catheter. To obtain adequate sensitivity for measurement of low urethral pressures, capacitive sensors with small micron-sized air-gaps on a flexible substrate are utilized. With capacitive sensors, stray fringe capacitance from human tissues is a significant source of error. This error is removed by using both a reference sensor that is insensitive to pressure but measures stray capacitance only and by using a Faraday cage that covers all the sensing elements and almost separates the electrical field inside the sensing capacitive elements from outside.

The proposed technique provides real-time measurement of the distribution of pressure and can be used for urethral measurement during provocative maneuvers, such as coughing, pressing the stomach, etc.

1.5 Major Contributions

1- Biomedical pressure sensors have previously been developed in literature for cardiac, eye and brain applications [47], [48], [49]. However, these applications involve only a single sensor, and not a series of pressure sensors on a flexible substrate for distributed force measurement. The urological domain has never previously been addressed through the development of micro-sensors for clinical applications.

2- This thesis develops a new ex-vivo validation procedure to verify the performance of the new instrumented urethral catheter.
3- Other existing sensors can only measure average circumferential pressure at a single point in the urethra. No other existing sensors can measure dynamic changes in pressure and the urethral pressure profile along the length of the urethra during provocative maneuvers such as coughing and Valsalva.
4- Faraday cage: The thesis develops a thin and transparent outer layer of gold to separate electrical fields outside the capacitive sensing elements from inside to significantly reduce the stray capacitance and enhance the signal to noise ratio. This gold layer is ultra-thin to decrease the effect of adding mechanical stiffness to the sensing element and keep the sensitivity high enough to reach the sensor resolution and range of interest.
5- Compensation of stray capacitance: This thesis develops a method of compensation for stray capacitance by using reference sensors that measure capacitance due to the environment but are uninfluenced by force or pressure variables.

Chapter 2

2 SENSOR FABRICATION

2.1 Sensor Design

Pressure inside the urethra for a healthy adult varies from zero at the orifice opening to a typical maximum value of ~100 cmH_2O somewhere close to the middle and beneath the sphincter muscle (Figure 3) [50]. The desired pressure measurement resolution specification for the sensors on the catheter is 5 cmH_2O. A capacitive pressure sensing mechanism is selected to get tiny sensors with high sensitivity, high flexibility and robustness against temperature changes [20]. An array of 9 individual sensors is proposed with 5 mm spatial resolution along 4 cm, which is the average length for an adult female human's urethra.

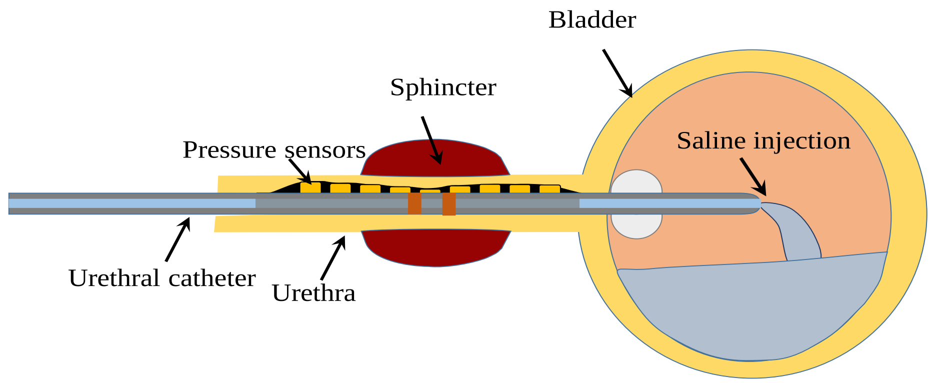

Figure 3: Instrumented catheter with sensors. The Foley retention balloon helps the catheter stay inside the urethra.

The width of the strip is 2 mm and it can be placed on 7 Fr (and above) Foley catheters. We placed our sensor on a 7 Fr

Foley catheter (TDOC-7FSC) for testing purposes. To use the maximum available space on the catheter, the width of each capacitive sensor on the strip is chosen to be 400 µm and the length to be 3.64 mm to accommodate 9 sensors in the urethra (Figure 4).

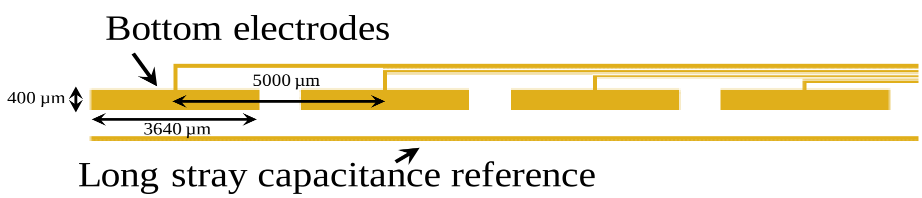

Figure 4: Sensing element's dimensions.

2.2 Modeling of the Capacitive Pressure Transducer

A capacitive sensor is the basic pressure measurement sensing unit utilized as part of an array in this project. There are two electrodes in the capacitive sensor, one on top and the other one on the bottom. In the schematic in Figure 5, a sensing electrode is at the bottom of the sensor under a dielectric. The top electrode is the common ground plate for all the sensors. The deflection of the top electrode causes the distance between the electrodes and hence the capacitance of the sensor to change, after which the capacitance change can be measured and can be converted back into pressure readout.

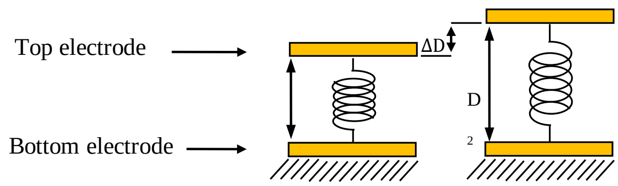

Figure 5: Mechanical model of a capacitive pressure transducer.

If the distance between the electrodes is changed by applying a normal force on them, then the capacitance changes. The sensitivity of capacitance change to the applied pressure can be calculated as follows [51]:

$$C = \frac{\varepsilon_0 \varepsilon_r A}{D} \tag{1}$$

$$\Delta C \cong -\varepsilon_0 \varepsilon_r A \left(\frac{\Delta D}{D^2}\right) \tag{2}$$

where ε_0 is the permittivity of air which is 8.85×10^{-12} F/m, A is the common area of the plates and D is the distance between them.

From static equilibrium of the top electrode under a deflection ΔD due to a pressure ΔP, the sensitivity of the sensor can be found as follows

$$S = \frac{\Delta C}{\Delta P} \cong -\varepsilon_0 \left(\frac{\varepsilon_r}{\kappa}\right)\left(\frac{A^2}{D^2}\right) \tag{3}$$

where k is the stiffness of the top electrode and S is the sensitivity of the sensor and shows the change in capacitance due to change in applied pressure. The sensitivity depends on the stiffness of the deformable electrode. To estimate the stiffness, k, of an individual sensor, the electrode is modeled as a clamped copper rectangular membrane under uniform pressure p, as shown in Figure 6.

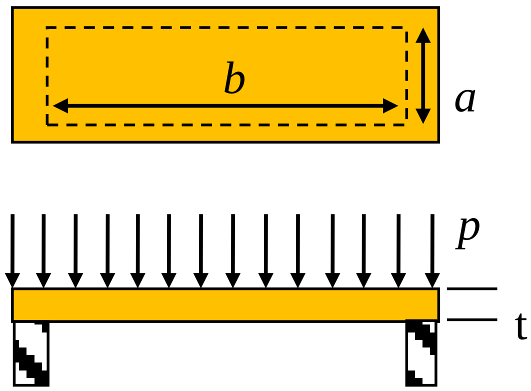

Figure 6: Mechanical model of a capacitor's electrode.

The maximum deflection of rectangular diaphragms is at the center [52] and is

$$y_m = \frac{0.0284pb^4}{Et^3\left(1.056\left(\frac{b}{a}\right)^5 + 1\right)} \tag{4}$$

where p is the applied pressure, a is the dimension of shorter edge, b is the dimension of the longer edge, t is the diaphragm thickness and E is the modulus of elasticity of the structural material. Since the total distance between top and bottom electrode is just 10 µm, while the lateral dimensions of each top electrode is 400 µm × 3644 µm, it is assumed that the deformation of the membrane is linear (Figure 7). Indeed, the central deflection from equation (4) is found to be less than 1 micron even for maximum pressure. The approximate capacitance change due to applied pressure can then be calculated as follows.

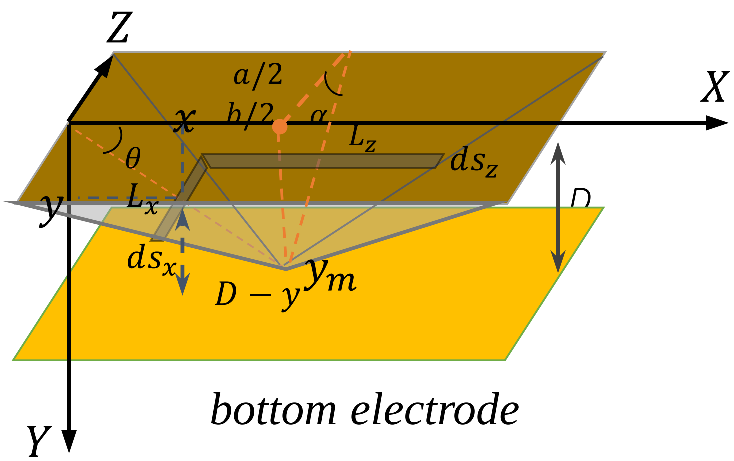

Figure 7: Top electrode is assumed to deflect linearly due to applied pressure.

The total capacitance after pressure is applied is the integral of the infinitesimal capacitors shown in Figure 7, integrated over the area of the plate. The calculation of the total capacitance is shown in equation (5).

$$C = 2\int \frac{\varepsilon L_x}{cos\theta} \frac{dx}{D - \frac{2y_m}{b}x} + 2\int \frac{\varepsilon L_z}{cos\alpha} \frac{dz}{D - \frac{2y_m}{a}z} \tag{5}$$

where $cos\theta = b/(2\sqrt{(b/2)^2 + y_m^2})$ and $cos\alpha = a/(2\sqrt{(a/2)^2 + y_m^2})$. To find the order of capacitance change, the sensor design parameters D =10 μm, $\varepsilon_r = 1$, ΔP=0.1 psi and E_{copper} = 17.0×10^6 psi for copper electrode should be plugged into equations (4) and (5), and that gives y_m = 30 nm and $\Delta C \cong 3.6$ fF. Thus, the theoretical sensor sensitivity is expected to be 36 fF/psi. This level of capacitance change can be easily measured using commercial capacitance measurement chips.

This analysis has shown that a sensitivity capable of measuring 0.1 psi can be achieved by each of the sensors in the strip. Equation (3) can be rewritten as

$$S = -\varepsilon_0 \lambda \beta^2 \qquad (6)$$

where λ is a material parameter that is the ratio of electrical permittivity to mechanical stiffness and β is a geometric parameter and is the ratio of the common area of the electrodes to their relative distance. To improve sensitivity, λ and β need to be made as high as possible.

2.3 Fabrication Process of the Sensing Strip

The electronics for the capacitance to digital converter (CDC) chip are incorporated directly on the sensing strip to measure the capacitance and digitize the data on the catheter right next to the sensors, thus preventing addition of noise during signal transmission and for having a robust mechanical connection to the chip and later to the computer. Further, a custom test and validation process is developed to test the actual urethral measurement ability of the catheter using an ex-vivo sheep bladder and urethra. Finally, the ability of the system to compensate for tissue stray capacitance and measure absolute urethral pressures accurately is verified, by using a reference stray capacitance transducer and a compensation algorithm.

A flexible sensing strip with 9 capacitive force sensors on it is fabricated. Being an ultra-thin flexible sensing strip, it can be adhered to catheters that can be used in urology, endoscopy and other in vivo applications. The flexible capacitive pressure sensing strip is made of three separate layers: top, middle and bottom. The top and bottom electrodes contain copper electrode on a polyimide substrate while the middle polymer layer serves as the glue and separator between the top and bottom electrodes. The schematic of an individual capacitive sensor on this sensing strip is shown in Figure 8.

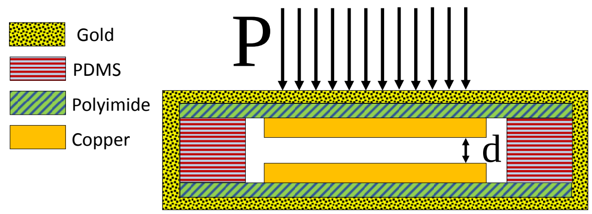

Figure 8: Structure of each capacitive pressure sensor: top and bottom electrodes are etched into 9 µm copper on polyimide substrate, distance between the electrodes is kept by middle PDMS layer.

A photograph of the fully fabricated sensing strip with all 9 sensors on it is shown in Figure 9. The overall dimensions of the top layer of electrodes in the sensing strip is approximately 7 cm × 3 mm, with micro-fabricated built in features inside each sensor of 20 µm resolution. The electrodes on both top and bottom layers are created by using a substrate of polyimide with pre-deposited copper on it, purchased from DuPont (AC091200EV from DuPont Flexible Circuit Materials Group). The 9 µm thick copper on the 12 µm polyimide substrate is patterned to create both the top and bottom electrodes as well as the circuitry for the CDC chip. The CDC chip and associated electronic components are integrated with the sensing strip to reduce the length of the traces between the sensing electrodes and the chip. This will decrease the amount of stray capacitance and also avoids having a separate connector device in between the sensor strip and the chip, as shown in Figure 9. Using a connector between the sensor and chip not only adds noise to the signal, but moreover adds stress concentrations in the flexible substrate that can break the sensor during in vivo insertion. PDMS (Sylgard 184) is used to make the middle layer which is the structure between top and bottom layers to keep the distance between the top and bottom electrodes (Figure 8). The high flexibility of the assembled sensing strip allows it to be mounted on catheters for recording pressure distribution in real time inside body's cavities and in between tissues.

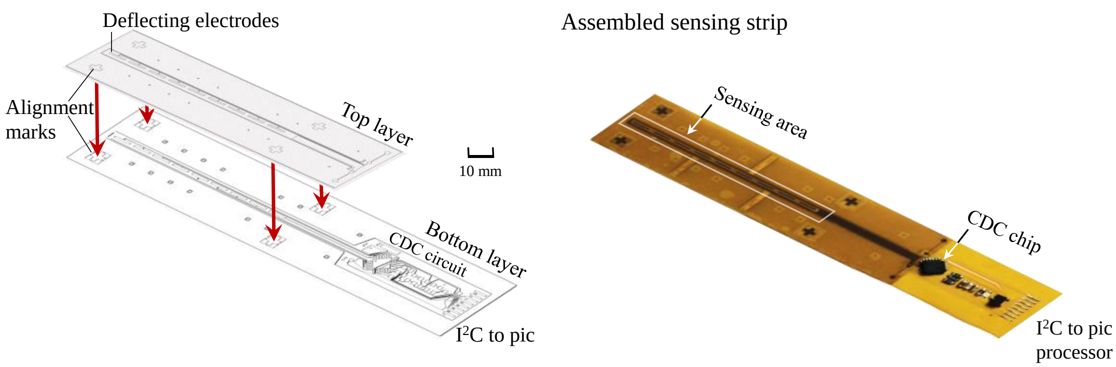

(a) (b)

Figure 9: (a) Top and bottom layers of the sensing strip, (b) Assembled sensing strip with 9 pressure sensors.

To make a Faraday cage for protecting the capacitive signal due to pressure from stray capacitance, the deposition of a thin enclosing layer of highly conductive metal, such as gold (resistivity = $2.44\times10^{-8}\ \Omega.m$), is needed. However, when the three layers need to be assembled together to create the sensor, they should be aligned accurately with respect to each and then bonded to make the sensing strip. Deposition of gold after the sensor has already been assembled can be considered. However, since deposition of gold in a thermal evaporating machine (Figure 10) happens in near-vacuum at very low pressure (1.3 $\times 10^{-6}$ Torr), it is highly risky to place the assembled sensing strip in an evaporating machine to deposit the conductive film on it. The air that is encapsulated inside the individual sensors will expand under vacuum and could delaminate the assembled sensing strip. Hence, the Faraday cage had to be fabricated and included on the outer surfaces of both the top and bottom electrode layers *before* assembly. The Faraday cage then had to be made transparent to be able to see the alignment marks on the three layers for assembling the layers. To achieve transparency in the gold layer, it was etched to create a gold mesh through which the underlying layers are visible. The mesh is designed to have a continuous array of openings of size 60×60 μm^2 to make the Faraday continuous and conductive, but at the same transparent.

Figure 10: CHA evaporator, the silver chamber at right is where the metal is evaporated and then deposited on the samples.

First the Faraday cage in gold is made on the backside of the polyimide substrate. Then on the copper side of the polyimide substrate the electrodes are made (Figure 11). For gold deposition, the polyimide layer is AMI cleaned and baked to evaporate the residual humidity. Then a 20 nm adhesion layer of Ti is deposited on the backside of polyimide in a CHA evaporator machine followed by deposition of 400 nm gold (Figure 12a). The bonding strength of gold and polyimide can be verified by sticking and peeling of a Kapton tape.

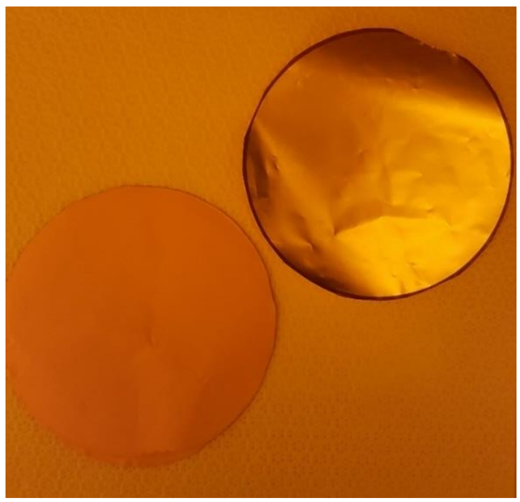

Figure 11: Left 9 um copper on PI, right is 400 nm gold on 20 nm titanium.

The fabrication of the Faraday cage then continues by transferring the sample onto a PET substrate (Grafix Clear .005 Dura-Lar Film). This substrate choice helps in cutting out the sensor and at the same time provides optical transparency which is important later in the alignment of the top and bottom electrodes during assembly. A water-soluble glue is used to fix the sample on the PET substrate. Then to pattern the Faraday cage, a masking layer from s1813 photoresist is made by photolithography techniques. The masking layer is a mesh with tiny square shape windows of $60\times60\ \mu m^2$ and trace thickness of 30 µm. Then the setup is immersed in gold etchant GE6 for 30 sec followed by BOE

(Buffered Oxide Etch) 10:1 for 10 sec to etch and pattern Ti under the gold layer. Finally, the s1813 masking layer is peeled off in acetone.

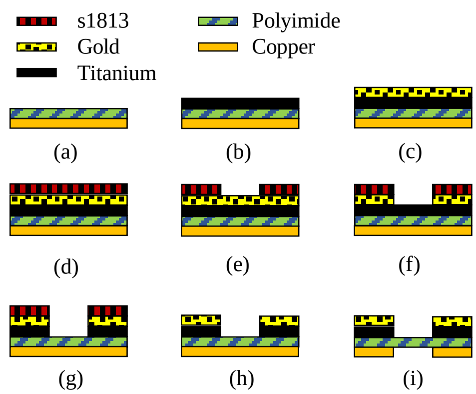

(a)

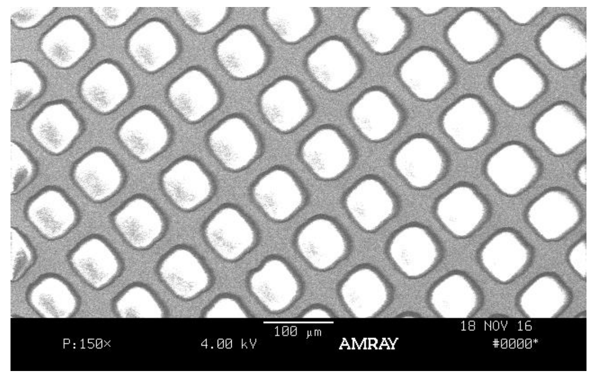

(b)

Figure 12: a) Fabrication steps of the Faraday cage, b) SEM image of the fabricated transparent Faraday cage: dark area is gold and bright area is polyimide.

The Faraday cage needs to be connected to the alternating voltage of the sensing CDC chip and needs to be further covered by an insulation layer should be insulated. So, after bonding together the top and bottom layers, the polymer PDMS is further coated and cured on the Faraday cage.

After fabrication of the Faraday cage the sample is flipped and placed on the PET again and fixed with small drops of a water-soluble glue. Now the sensors and signal lines are made of copper on a polyimide sheet (Figure 13) with 9 µm electro deposited copper (AC091200EV from DuPont Flexible Circuit Materials Group). Patterning of the copper layer to create the electrodes is initiated by coating copper by 2 µm photoresist 1813 (MicroChem Corporation). Due to the thermal expansion coefficient being higher for copper than the polyimide and PET layers, the setup cannot withstand temperature higher than 70˚C. Otherwise the copper layer will expand more than the polymer layers and everything will irreversibly deform. Hence, the standard operating procedure for curing photoresist 1813 is changed to soft baking at 65˚C for 3 min and hard baking at 65˚C for 15 min after photolithography. The electrodes and traces were then made by submerging it into copper etchant $FeCl_3$: H2O 1:8 (v/v) (MG Chemicals 415 Ferric Chloride Liquid), at 500C in the solution for 40 min. The Copper etch rate is about 225 nm/min in this solution. Subsequently, the photoresist 1813 is washed out in acetone and the electrodes were checked under microscope and tested with a multi-meter to ensure the integrity of all signal lines and electrodes.

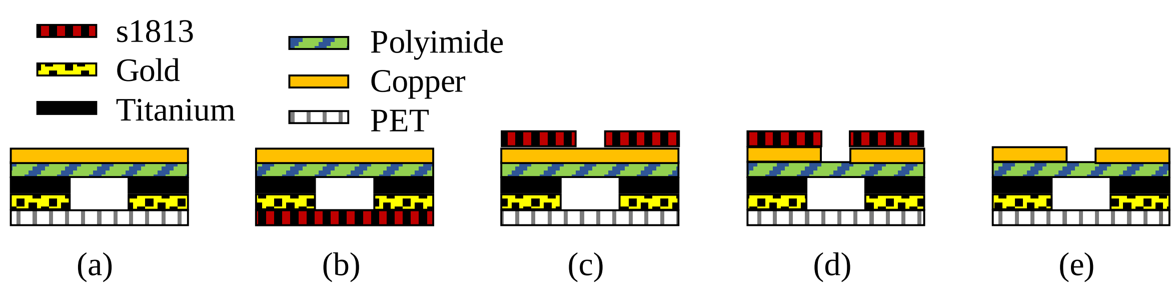

Figure 13: Electrode fabrication steps.

The fabricated copper electrodes are shown in Figure 14.

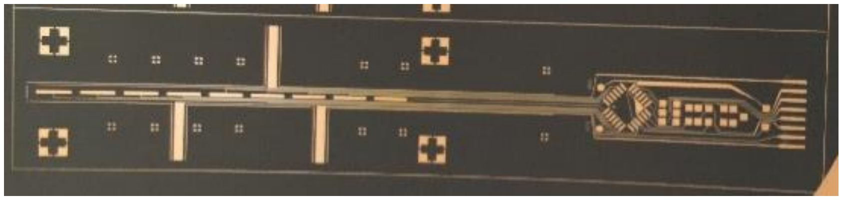

(a)

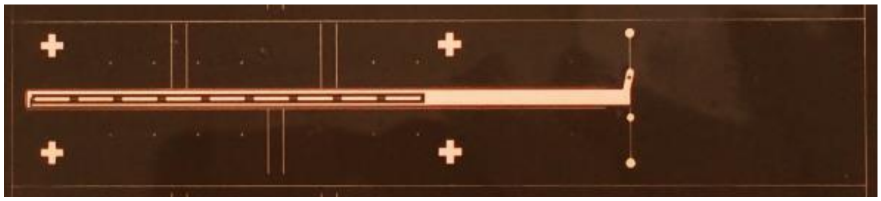

(b)

Figure 14: a) Fabricated bottom electrode and CDC circuit, b) Top electrodes.

After fabrication of the top and bottom copper electrodes, a spacer layer from PDMS (Sylgard 184, Dow Corning) is made to hold the structure of the sensor together. PDMS is utilized for this purpose because it is transparent and flexible. For the spacer layer, PDMS is spun on both top and bottom electrodes separately. The thickness on the bottom electrode is 5 µm. This layer will prevent any short circuits between top and bottom electrodes in the case of exceeding the designed pressure range. The thickness on the top electrode is 5 µm for making the air cavity layer to allow deformation between top and bottom electrodes. After coating the electrodes with PDMS, they were placed on a hotplate at 65˚C for 3 hours for to cure on polyimide layer (Figure 16). After this step, photoresist AZ9260 is spun, baked and patterned on PDMS to make a masking layer. The thickness of AZ9260 is 20 µm. Soft bake is at 70˚C for 3 min with no hard bake. To make the 5 µm cavity, PDMS layer on top electrode is fully etched by plasma (Figure 15) in the STS etch machine (SF6, 45 sccm, O2, 15 sccm, 100 mTorr, 100 W). The etching rate is 150 nm/min. After checking the etched profile with the surface profiler, they were washed in AMI to remove the photoresist and then put in oxygen plasma (O2:75 sccm, 100 W) to clean the PDMS surface and prepare them for bonding.

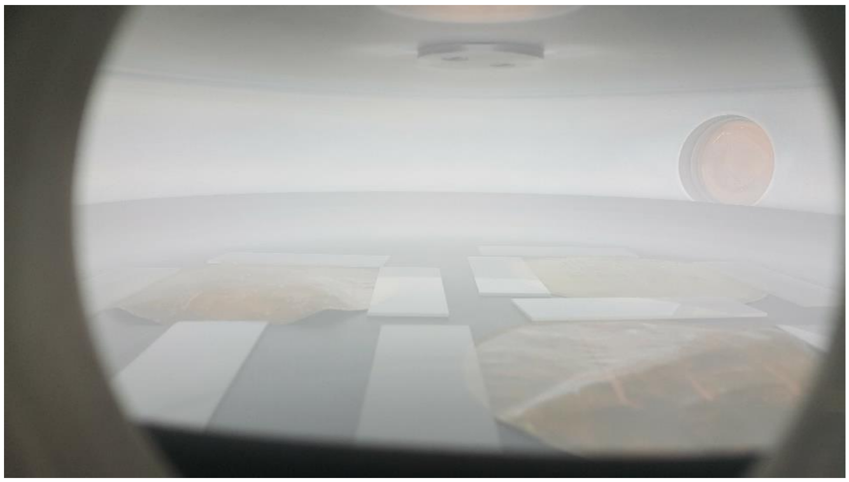

Figure 15: Samples in plasma to etch the PDMS layer (the purple light is coming from Oxygen plasma).

Alignment between top and bottom electrode-PDMS assemblies is done within 10 min, otherwise the surface had been treated by oxygen plasma again.

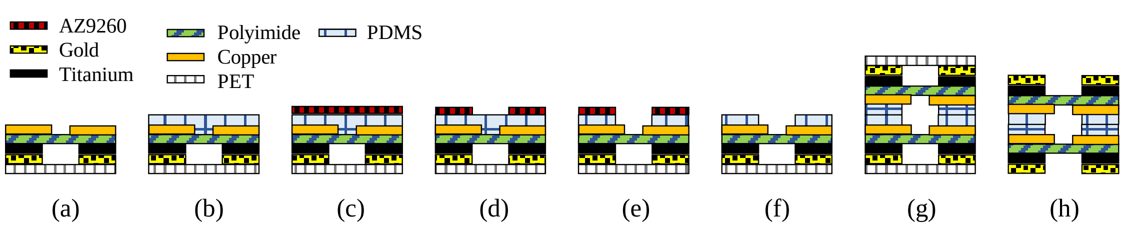

Figure 16: Sensor fabrication steps.

In Figure 17 one capacitive pressure sensing element is shown after assembly.

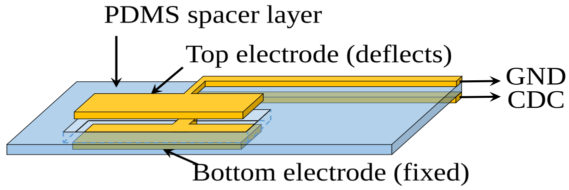

Figure 17: One pressure sensing element after assembly.

Three different shapes for the top electrode were designed and fabricated to find the best one that meets the sensitivity requirements. The three shapes are the spring shaped electrode, the elliptical electrode and the rectangular electrode, as shown in the photographs in Figure 18.The spring shaped and elliptical electrodes have less metal and were therefore expected to be less stiff compared to the rectangular electrodes. However, the rectangular electrode has more metallic surface area and therefore more electrical sensitivity. In addition to the metal, the top electrode has a polyimide substrate and hence the stiffness reduction achieved by reducing metal is limited.

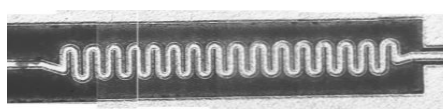

(a)

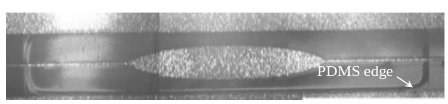

(b)

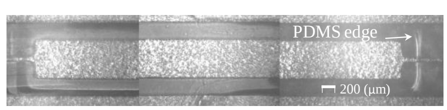

(c)

Figure 18: Three fabricated designs for top electrode: (a) spring shaped, (b) elliptical: a dashed rectangle is drawn to show the etched window in PDMS, (c) rectangular. PDMS cavity can be seen in (b) and (c).

The top common ground electrode contacts a ground trace line on the bottom substrate through conductive epoxy after the PDMS-top-electrode structure is flip-chip assembled on the sensor strip (Figure 19).

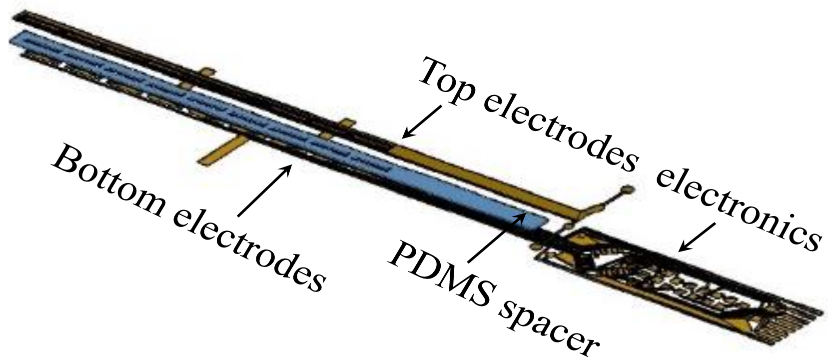

Figure 19: Assembly of layers of the flexible sensing strip.

A four degree of freedom aligner is constructed for the aligning steps (Figure 20). Since the electrodes are flexible, they may easily wrinkle and create small waves on top of the substrate. Wrinkles can produce variability in the sensor resolution and range. Hence an aligner is made to hold the top and bottom electrodes using vacuum. The bottom stage can move in x and y directions and rotate around the z axis while the top electrode just moves in the z direction. Backlight through the bottom is provided by blue LEDs to see through the sensor. This is possible because of the polyimide and PDMS layers being translucent. So, the alignment marks are visible if there is enough light from the bottom of the aligner. After careful lining, up of the alignment marks and pressing the top and bottom layers slightly together, the vacuum is released.

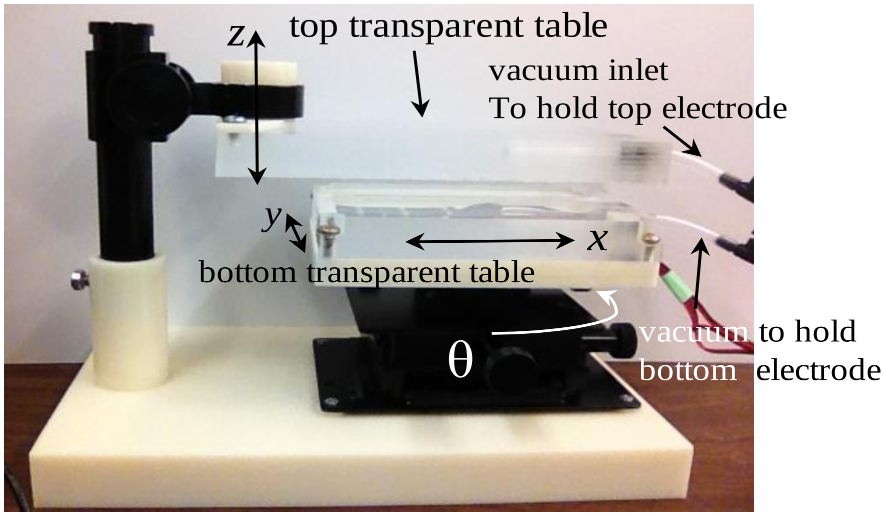

(a)

(b)

Figure 20: a) A 4 degree of freedom custom made aligner setup, b) Top view of aligned electrodes.

Then the whole setup is placed between two glassware slides and set on a hotplate at 90˚C for 10 hours overnight. Two 100 g calibrating weights were put on the glassware slide to provide uniform pressure for PDMS to PDMS bonding for 12 hours (Figure 21).

Figure 21: Bonding top and bottom layers on a hotplate.

After verifying good connections between the top electrode and ground signal the electrical components for capacitance measurement are installed and soldered (Figure 22). The 16 bit capacitance to digital converter AD7147 (AnalogDevice) that reads the capacitance in the range of ± 8 pF. This chip sends the digital data serially via I^2C to a central microcontroller (pic16f1823) on a detachable data acquisition card. The sampling frequency is 10 Hz and every sample contains capacitance readings from 12 channels.

Figure 22: Assembled capacitive pressure sensing strip.

After the sensor is assembled it is cut (Figure 24) out using a custom-made laser cutting setup (2W 445nm LD module with 405-G-2 glass lens).

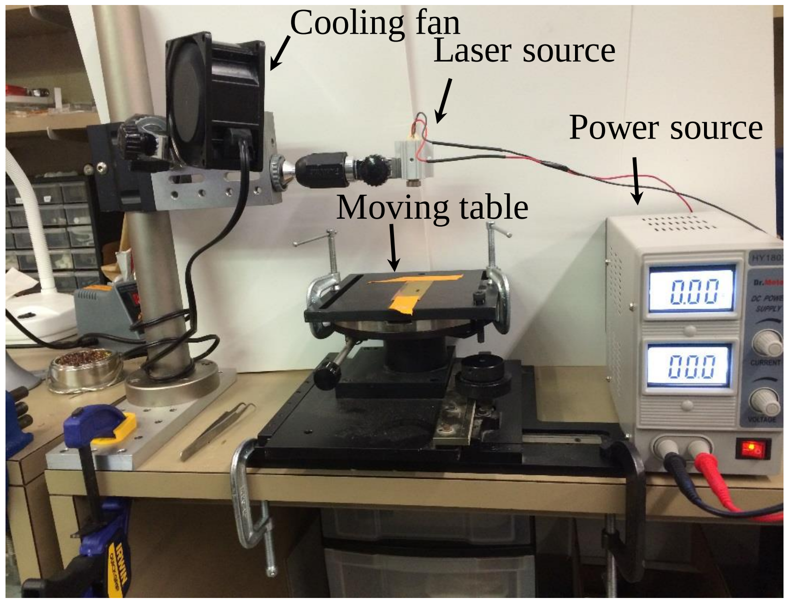

Figure 23: Manual laser cutter setup.

A 4 Volt input is enough to cut the 24-micron polyimide plus ~10 micron of PDMS. For final installation of the sensor on the catheter a supporting block of PDMS is molded around the catheter. This increases the real size of the catheter from 7 Fr to 8 Fr. The sensor strip is fixed on this supporting layer by curing a brushed layer of PDMS on it. The setup is left in water for several hours to verify the sealing quality and ensure its imperviousness to liquid.

Figure 24: Sensing strip cut out with laser.

In the last step before mounting the sensing strip on the catheter the connections are checked to make sure that the Faraday cage is working and gets the active square wave signal with 3.3 V amplitude and 250 kHz (Figure 25).

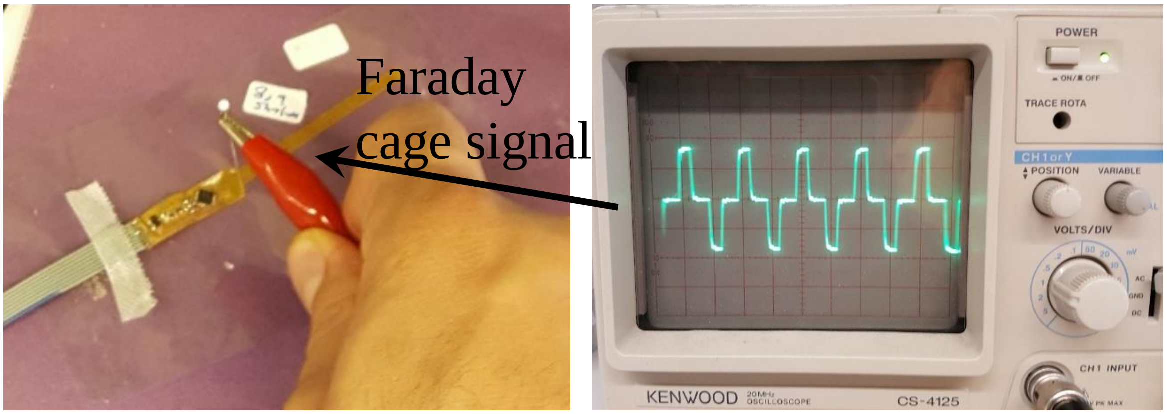

Figure 25: a) Testing the signal on the outer layer of the strip using a probe, b) The active shielding signal.

A 7 Fr Foley catheter is used as the device to be instrumented. The catheter has three separate lumens from the beginning all the way down the length of the catheter to the ending point inside bladder (Figure 26): one semi square shape lumen ($1100\times1100 \mu m^2$) that is open at both ends, and allows urine to drain out into a collection bag and two small and circular lumens (diameter 100 μm) that connect to a balloon at the tip. The balloon is inflated with air when it is inside the bladder to prevent the catheter from coming out of the bladder.

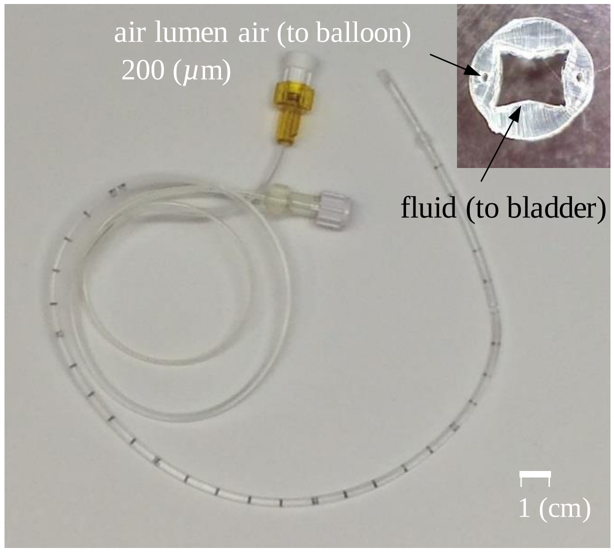

Figure 26: a) Foley catheter, b) cross sectional view of the catheter.

To install the sensor array on the catheter, a rectangular block from PDMS (transparent and flexible) is fabricated around the catheter by molding. PDMS is used to stick the micro-fabricated sensor to the flat surface (Figure 27).

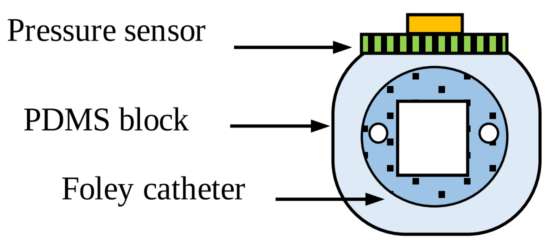

Figure 27: Schematics of the sensor on the PDMS platform on the catheter.

To do this a mold is designed and then fabricated by a 3d printer. The mold has two parts that come on the sides of the catheter. Then the two parts are pushed and kept tight together using two c-clamps. Liquid PDMS is injected into the mold from the inlet (Figure 28) and fills the whole mold. It creates a support for the sensing part of the fabricated sensors and the integrated flexible circuit that comes with it.

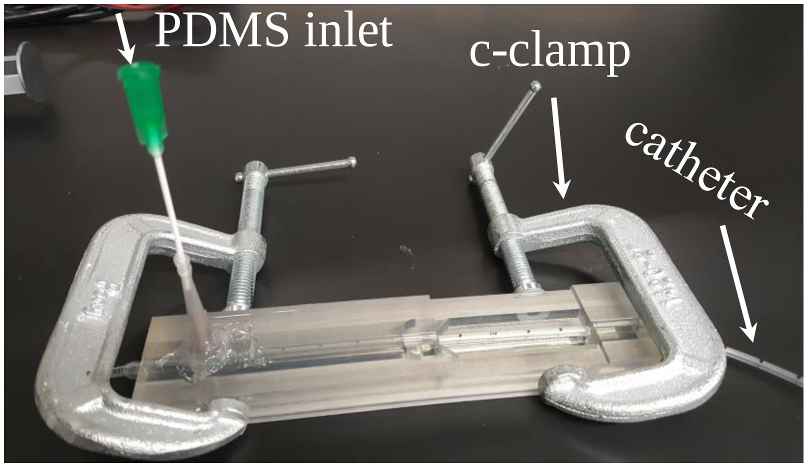

Figure 28: Molding PDMS to make the platform around the catheter.

The setup then is placed on a hotplate at 90˚C for 4 hours to cure the PDMS. After removing the mold a flexible platform is ready to install the fabricated sensing strip (Figure 29).

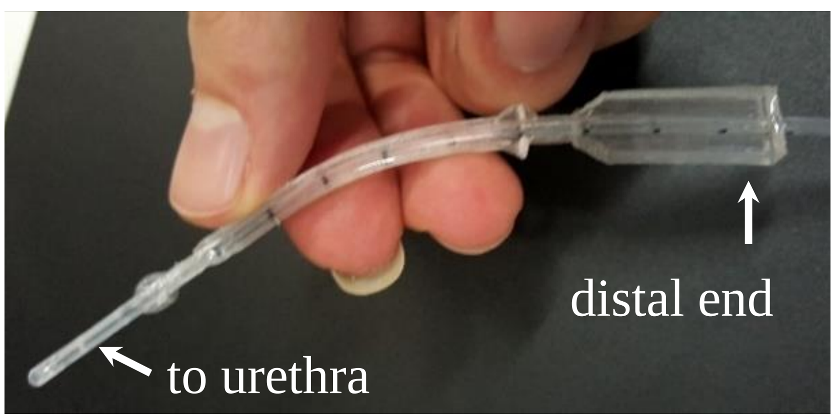

Figure 29: Flexible PDMS platform molded around the urethral catheter.

Note that the sensor may be significantly bent during insertion, but once located in the urethra for data acquisition is expected to be relatively straight.

Figure 30: Sensor assembly: a) PDMS ground molded around the catheter, b) sensor strip fixed on a 7 Fr urethral catheter.

The last step in making the sensing catheter ready is to make and install a bump layer on the sensing elements. This helps to transmit the contact pressure from the tissue to the sensing element and increase the sensitivity of the sensors. A mold is designed in CAD software and printed by a 3d printer (Figure 31). Since the whole device is transparent the bump layer is aligned and bonded to the sensing strip using a silicon based glue.

Figure 31: Mold and fabricated bump layer.

A picture of the fully assembled sensing strip is shown in Figure 32.

Figure 32: Fully assembled sensing catheter.

The interface between the PI and PDMS layers does not get damaged by bending or by contact with liquid. The sensing strip has been immersed in saline for several hours to test the strength of the PI-PDMS adhesion. It is found that the layers do not delaminate even after several hours of immersion in saline. It should be noted that the sensors are meant to be disposable and one-time use only.

2.4 Sensor Packaging for Urethral Insertion

During the catheterization (insertion), the catheter experiences a combination of different loads such as buckling, torsion and bending. To protect the sensors from this complex loading we designed and fabricated a special handle that can hold the device during the catheterization and protect it against failure. Different designs for the handle are shown in Figure 33.

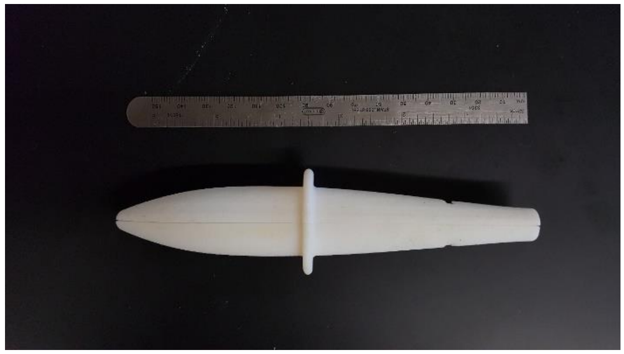

(a)

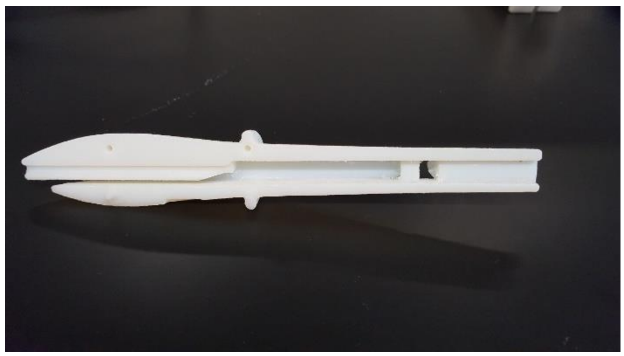

(b)

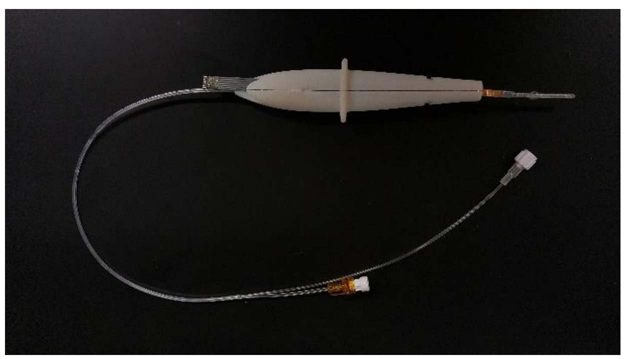

(c)

Figure 33: a) Printed handle top view, b) Printed handle side view, c) Handle holds the sensing catheter.

To protect the data acquisition card from moisture during the catheterization and the test, a package is designed and made by a 3d printer. It is designed to be self-assembled by pushing and holding the PCB in the right place. After assembly, it is sealed by sealing glue to protect the electronics from water during the test.

(a) (b) (c)

Figure 34: a) Data acquisition card, b) Printed package, c) Assembled data acquisition.

In Figure 35 you can see the evolutionary development of the sensing catheter and how it became smaller with time.

Figure 35: From left to right: the evolution of the sensing catheter.

Chapter 3

3 IN-VITRO AND EX-VIVO EXPERIMENTAL EVALUATION OF SENSORS

3.1 Calibration in Bench-Top Pressure Chamber

After the sensing strip is installed on a 7 Fr Foley catheter, it is first calibrated in an air pressure chamber (Figure 36). Also, a reference pressure sensor MS5534C manufactured by Intersema is placed inside the chamber for calibration purposes (resolution 7 cmH_2O). The sensitivity of sensors varies between 0.36 fF/cmH_2O to 0.64 fF/cmH_2O. The stray reference electrodes were not responding to applied pressure and responded only to stray capacitance. This behavior enables us to estimate the stray capacitance in the sensors and compensate for these stray capacitance to get the absolute pressure values inside the urethra correctly.

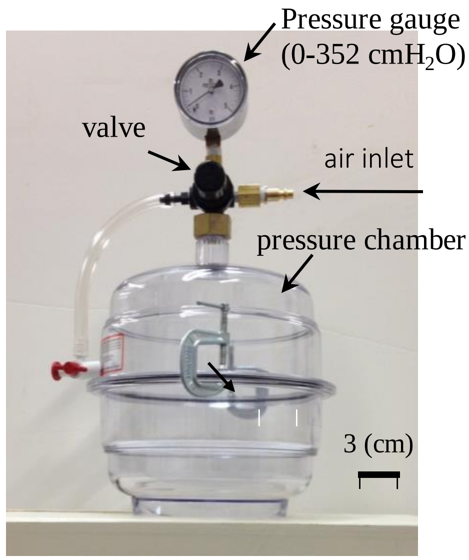

Figure 36: Pressure test setup to calibrate the sensing strip.

In Figure 37, the pressure is changed from 0 to 7 cmH_2O and it is observed that all 9 sensors respond to this small pressure change. In this figure, the capacitance change is shown on the vertical axis. The responses of the 9 sensors are not equal, varying from 1 fF for sensor 1 to 35 fF for sensor 8. This variability in sensitivity is expected to be due to unequal gaps obtained from the sensor assembly. Nonetheless, even the least sensitive sensor resolution is better than 0.1 psi. The difference in sensitivities can be eliminated by calibrating, so that all sensors provide readings in psi after calibration. The sampling time used is 170 milli-seconds.

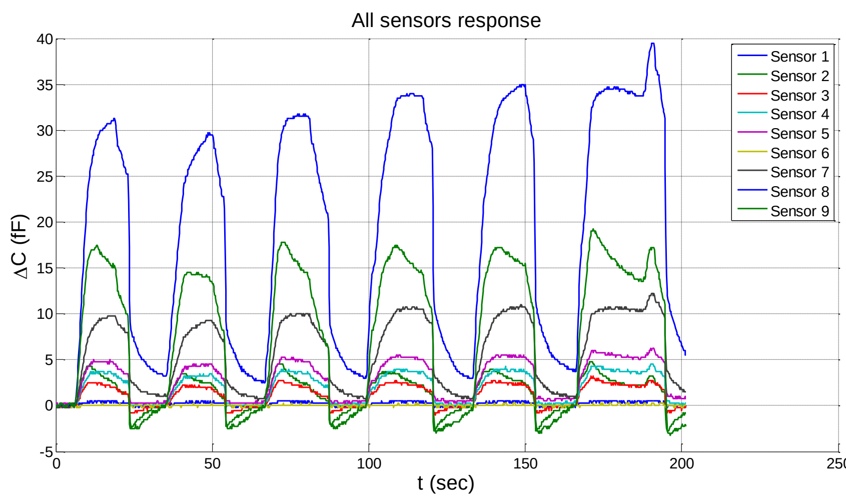

Figure 37: 5 tests, P = 7 cmH_2O sensors' response from C_1 to C_9.

The variation of capacitance with applied pressure is shown in Figure 38 for two types of electrodes – the rectangular and elliptical electrodes. The rectangular electrodes have more sensitivity but the elliptical electrodes in Figure 38b have more uniformity in the response of the 9 sensors, the calibration factor varying from 20fF/psi to 80 fF/psi. It should be noted that the analytical estimate of the calibration factor is 36 fF/psi.

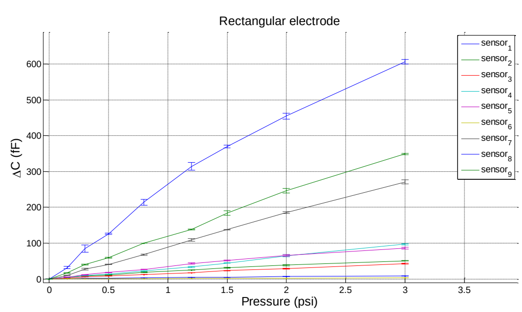

(a)

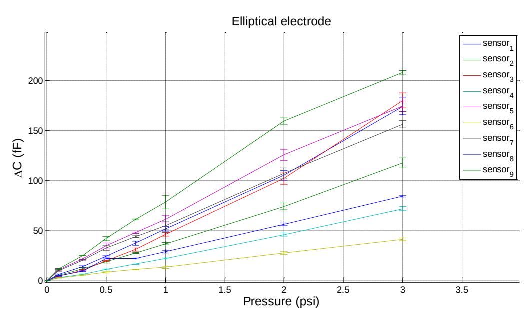

(b)

Figure 38: Sensor strip response (a) response of the 9 rectangular sensors to P=[0.15 0.3 0.5 0.8 1.2 1.5 2 3] (psi), five tests. (b) response of the 9 elliptical sensors to P=[0.15 0.3 0.5 0.8 1.2 1.5 2 3] (psi), five tests.

3.2 Ex-Vivo Experimental Setup

To verify the sensors' functionality before doing tests in real patients, the catheter is tested in a custom made ex-vivo setup (Figure 39). As described in the introduction, the validation of the instrumented catheter is a challenge due to lack of other gold standard sensors that can make distributed measurements in the urethra. The design of the custom designed test setup replicates the human lower urinary tract structure. The setup consists of three major parts (Figure 39): first, a rotating disk to set relative angle between cuff and the catheter. This enables us to get data at different angles and construct 3-dimensional pressure distribution circumferentially and longitudinally along the urethra.

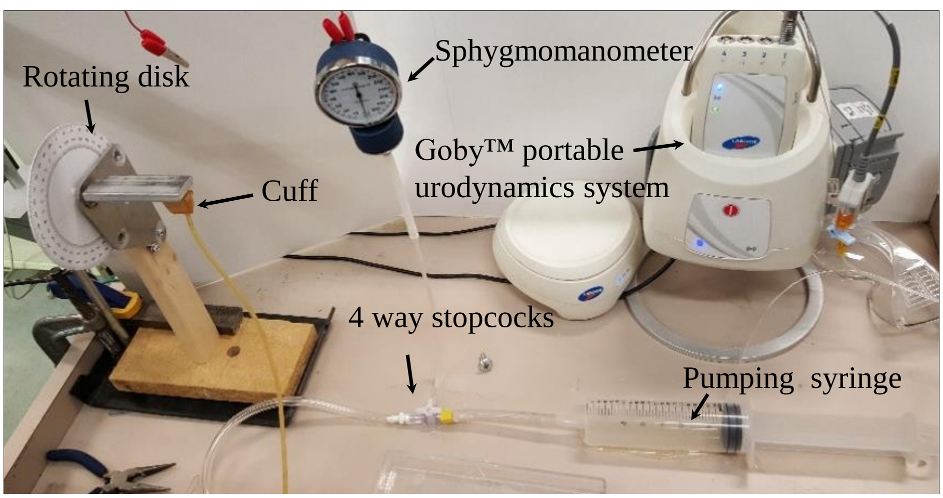

Figure 39: Ex-vivo test setup: side view of an extracted sheep's bladder and urethra

Second, a pneumatic circuit that consists of a 100 ml syringe (pump), a cuff (AMS 800 Urinary Control System Cuff) and sphygmomanometer is used. This cuff works as an artificial sphincter muscle and exerts pressure on outer part of the urethra. In addition, a sphygmomanometer is connected to the line to measure pressure inside the cuff. And finally, the third part of this test setup is a sheep's urethra that is extracted from lower urinary tract of a sacrificed sheep. This urethra transmits the cuff's pressure to the sensing catheter inside it (Figure 40).

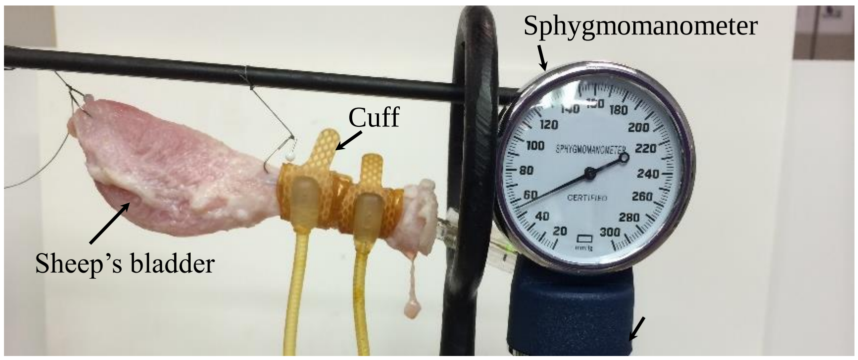

Figure 40: Test setup: cuff and urethra, cuff's pressure can be read from sphygmomanometer.

A Goby™ portable urodynamics system is also used that measures pressure inside the urethra using a single air charged balloon. A sheep's bladder and urethra were chosen as the ex vivo model because the sheep urethra is 4 cm long, like the female human urethra and the passage from the external body opening to the urethral opening is very short in a sheep, again like the female human anatomy.

3.3 Experimental Data: Measurement of Dynamic Pressure

The test procedure is performed as follows: the disk is fixed at angle zero, recording data starts when the catheter is in atmospheric pressure outside of the urethra. Then the sensing catheter is inserted into the sheep's urethra. The signal shifts at this point due to both stray capacitance created between sensing electrodes and the urethra plus some pressure exerted by urethral walls (Figure 41). Then the cuff is wrapped and locked around the urethra. Sensors 5 to 8 are under the cuff and respond to applied pressure while sensors 1 to 4 are not under the cuff and hence do not respond to cuff's pressure. At this point three different sequentially pressure values of 34 cmH_2O, 68 cmH_2O and 136 cmH_2O (each one for 3 times) are applied on the sensing area by the cuff. Then the cuff is opened and the disk is rotated by 30 deg and locked to repeat pressure test at the new angle. The sampling rate for recording real time data is 10 Hz. This is done until a complete data for every 30 deg around one revolution is obtained. Software in MATLAB is used to record and process the data.

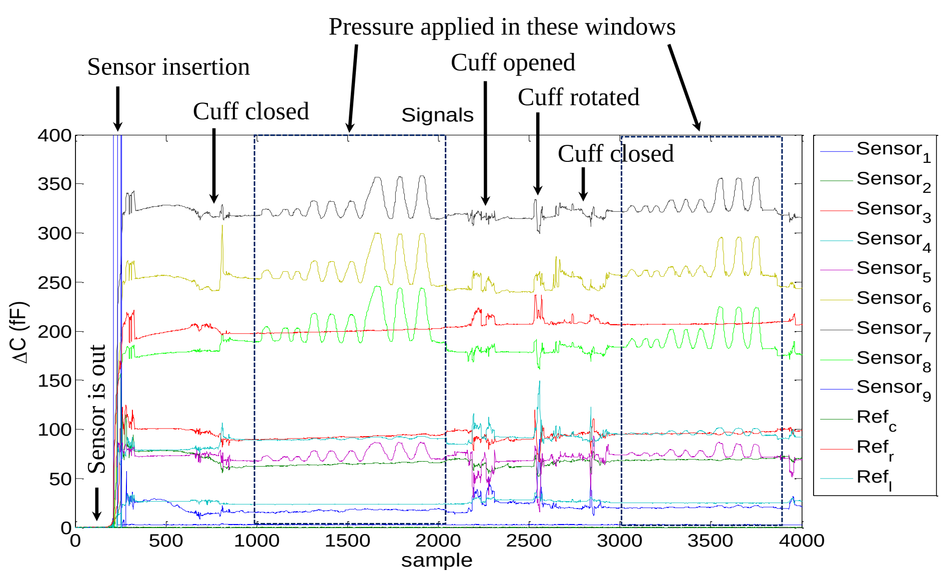

Figure 41: Sensors' responses to the cuff pressure: the enclosed regions by dashed rectangles are responses of the sensors to the cuff pressure at angles 0 and 30 deg.

The output signal from any single sensor is the summation of capacitance change due to applied pressure plus stray capacitance. This stray capacitance can be viewed as an additional capacitor working in parallel with the sensor:

$$S = \gamma P + N \tag{7}$$

where S is the measured output signal, γ is the calibration coefficient, P is the actual pressure that is unknown and N is the stray capacitance.

Two single electrodes are built in the sensor strip to obtain a real-time estimate of the stray capacitance. In the calibration of the sensing catheter in the pressure chamber we saw these electrodes do not respond to the applied pressure and are just sensitive to stray capacitance. So if the material around the sensors remains uniform and does not change then any change in the signal is related purely to change in cuff's pressure (Equation (8)).

$$\Delta S = \gamma \Delta P \tag{8}$$

To verify and calibrate the performance of the sensors the same tests were performed on an air-charged balloon sensor on a FOLEY catheter using a Goby™ portable urodynamics system. A 7 Fr FOLEY catheter is connected to the external pressure transducer and the balloon is partially charged as is mentioned in the manual. Because of the shape of this sensor the contact area of the sensor and the urethral wall will be cylindrical and pressure will be averaged on that area.

To compare the results of the new sensor and the air-charged balloon sensor, we measured pressure at different angles with the new sensor and calculated the average circumferential pressure. It should be noted that no circumferential variation in pressure at any one longitudinal location in the urethra is expected in a live animal. The circumferential changes in these ex vivo tests occurred due to use of an artificial cuff to provide urethral pressure. In Figure 42 the response to pressure change in the cuff is plotted against different angles and then integrated and compared with the value read from a 7 Fr commercial Foley catheter T-DOC7FS. The cross section of the cuff after inflation creates three connected chambers that are folded (Figure 42a) and hence the applied pressure distribution around the urethra is not uniform and varies between local minimums at the folded edges to maximums at the middle of the chambers. Three minimums corresponding to the three folded edges of the cuff can be seen in Figure 42b. They occur at angles 60 deg, 150 deg and 300 deg. Also three maximums related to inflated chambers can be identified at angles 0 deg, 120 deg and 210 deg. The difference between the average value of sensor 6 over different angles and the single reading from the air-charged balloon sensor is 1.96 cmH_2O for 34 cmH_2O inside the cuff. As the pressure is increased to 68 cmH_2O (Figure 42c) and 136 cmH_2O (Figure 42d) the difference between minimums and maximums is reduced. It is because in higher pressures the folded edges are partially inflated, that makes the pressure distribution more uniform.

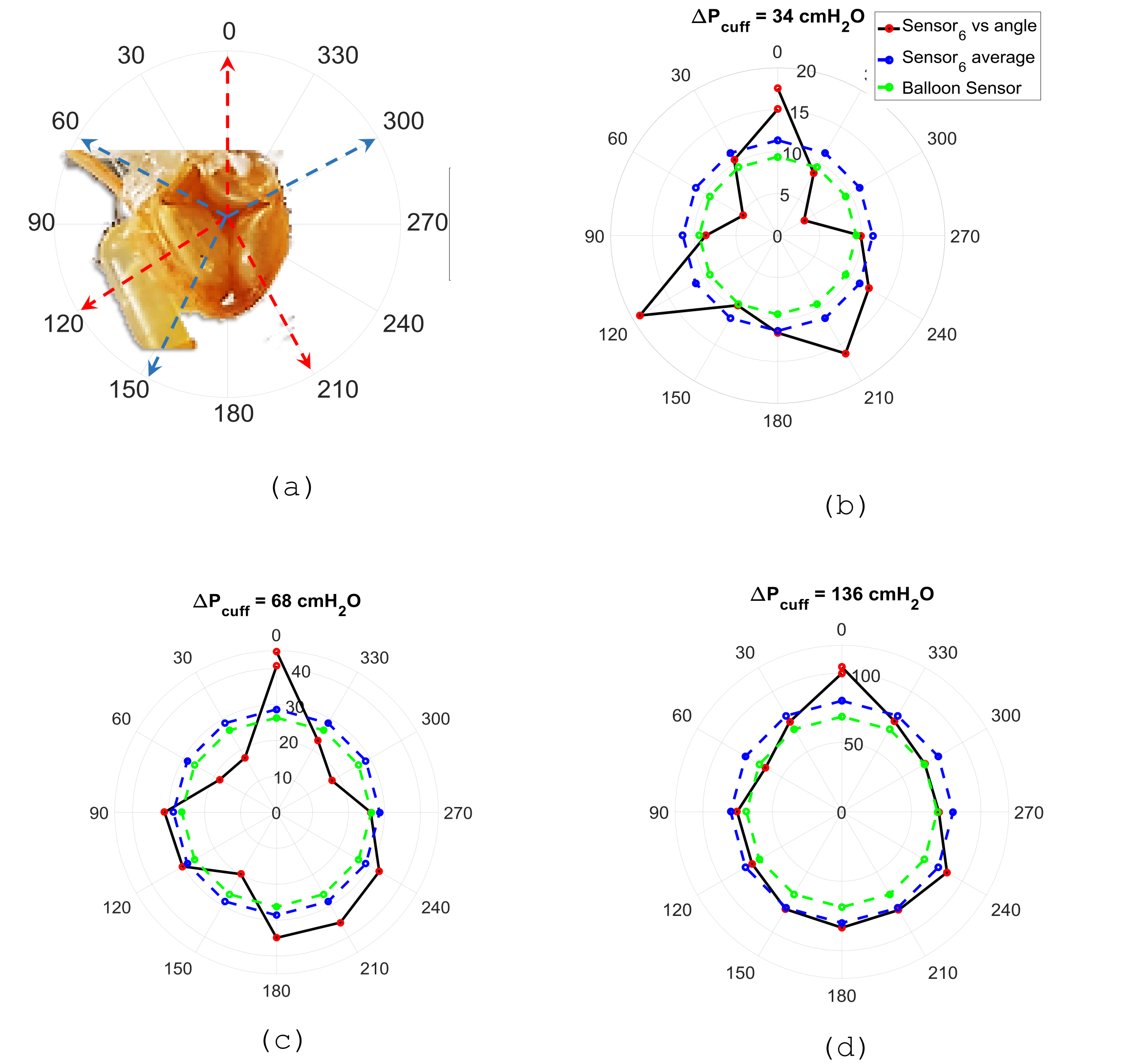

Figure 42: a) Cuff's cross section after inflation. The blue arrows show high pressure locations and the red ones point to the angle with low pressure, b) Sensor 6 response to ΔP=34 cmH2O at different angles and comparing the average value with air-charged balloon sensor, c) Sensor 6 response to ΔP=68 cmH2O at different angles, d) Sensor 6 response to ΔP=136 cmH2O at different angles.

3.4 Experimental Data: Stray Capacitance Compensation for Measurement of Absolute Pressure

To find the absolute pressure in Equation (7) the stray capacitance N should be removed from the signal (Equation (8)).

$$P = (S - N)/\gamma \quad (9)$$

Stray capacitance N is estimated in real-time by using the signals from the two single reference electrodes. It is assumed that N is proportional to the signal on the single electrode on the sensing strip (Equation (10)).

$$N = \theta R \quad (10)$$

where coefficient θ is an unknown constant multiplier and R is the stray capacitance signal that is measured by single electrode. Then θ can be calculated for every single sensor, if we have pressure measurement at different points in the urethra using Equation (10).

$$\theta = (S - \gamma P)/R \quad (11)$$

To find θ, pressure distribution inside the sheep's urethra is constructed point by point using Goby™ portable urodynamics system. This θ value can be used for cancellation of stray capacitance in later tests. This data is shown in Figure 43a. Calculated θ is presented in Figure 43b.

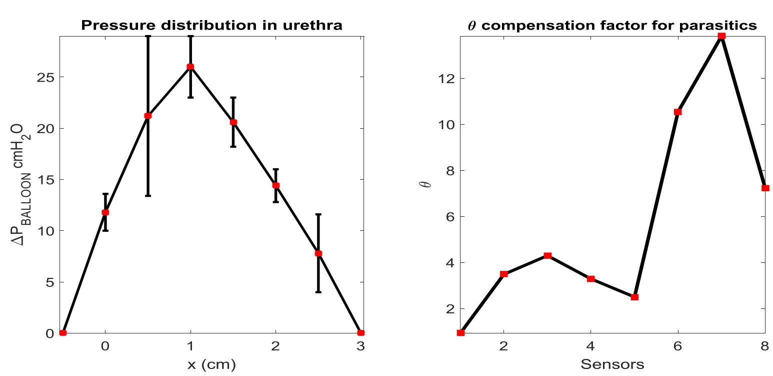

(a) (b)

Figure 43: a) Pressure distribution in sheep's urethra using a T-DOC single sensor catheter, b) θ values for every sensor on the catheter for stray capacitance compensation

Now that θ is found using equation (10), stray capacitance can be removed in real time from the signals and absolute pressure in the urethra can be calculated (Equation (12)):

$$P = (S - \theta R)/\gamma \tag{12}$$

3.5 Data Analysis and Verification

After stray capacitance removal, the absolute pressure can be calculated (Equation (12)) for the 9 sensors on the strip and plotted against position along the urethra to construct the UPP in the ex-vivo test setup. Reference pressure magnitude at different locations inside the urethra is measured point by point by using an air-charged balloon (TDOC-7FSC) that is connected to Goby™ portable urodynamics. To compare the results from the capacitive sensing strip with an air-charged balloon sensor the average value of each sensor's reading at different angles are taken.

Pressure distribution inside the urethra against the angle is plotted for sensor 6 on the sensing strip (Figure 44). The average value of these readings is taken and plotted with the reading from the balloon sensor. The difference between balloon sensor (reference) and the average value from our sensor is 0.96 cmH_2O, 2.33 cmH_2O and 5 cmH_2O for $\Delta P =$ 34 cmH_2O, $\Delta P =$ 68 cmH_2O and $\Delta P =$ 136 cmH_2O inside the cuff respectively. This also shows that the balloon sensors take the average of the pressure at different angles.

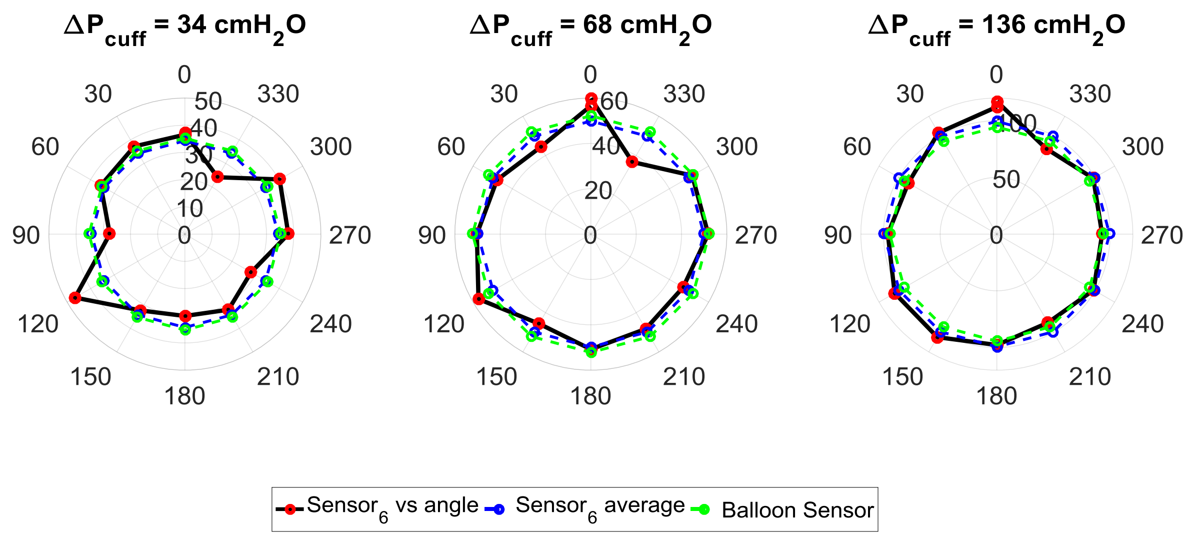

Figure 44: Pressure distribution in sheep's urethra using T-DOC single sensor catheter.

Placing the pressure-angle plots along the length of the urethra for the first time creates a 3 dimensional UPP that gives us pressure at different locations and angles inside the urethra (Figure 45).

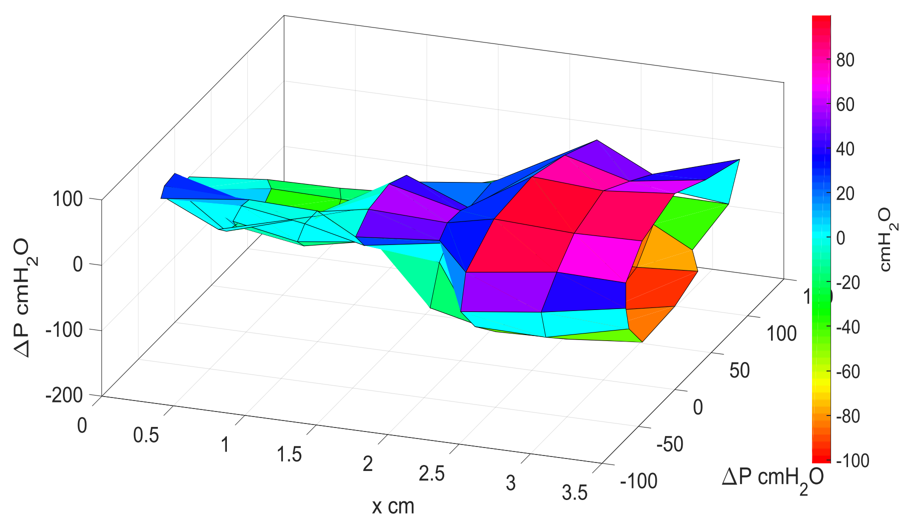

Figure 45: 3-Dimensional pressure distribution along the urethra for a cuff pressure equal to 136 cm H2O.

In Figure 46, pressure is averaged on the circumference and the result is plotted along the urethral length and compared with the balloon sensor's (T-DOC7FS) readout. The maximum of the averaged pressure is measured by sensor 6 at x = 2.5 cm. The result is pretty close and in the same order of the balloon sensor's measurement for different applied pressure values in the cuff.

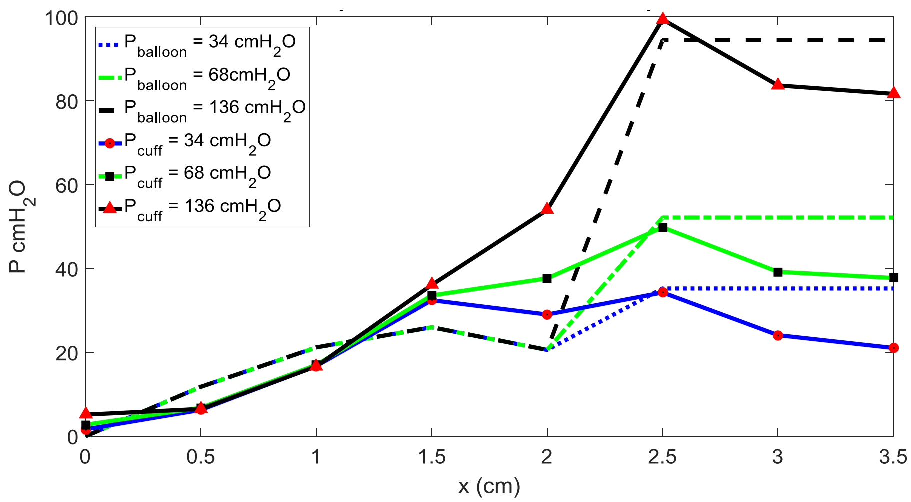

Figure 46: Absolute pressure distribution along the longitudinal direction of the sheep urethra.

Chapter 4

4 ACTIVE SHIELDING AGAINST STRAY CAPACITANCE

4.1 Faraday Cage and Stray Capacitance in Capacitive Pressure Sensors

It is well known from the time of Maxwell in 1873 that capacitance is created between any two electrodes with different electrical potentials:

$$C = \frac{Q}{\Delta V} \tag{13}$$

where C is capacitance, Q is the stored charge and ΔV is the potential difference of the electrodes. For a parallel plate capacitor with large electrode area, the electrical field will be almost uniform between the electrodes and Maxwell's definition of capacitance from equation (13) will lead to the following purely geometric definition of capacitance in Equation (14):

$$C = \frac{\epsilon A}{d} \tag{14}$$

where ϵ is the permittivity of the dielectric material, A is the common area between the electrodes and d is the distance between the electrodes. In Equation (14), the fringe electric fields at the edges of the plate are neglected. This assumption holds well when the common area between the electrodes is large enough. In real life, however, fringe electrical field outside the capacitor penetrates neighboring materials, as shown in Figure 47a and builds additional capacitance which is called stray capacitance. If the capacitor's lateral dimensions are not much larger than the distance between the electrodes, this stray capacitance cannot be ignored anymore. The latter is the case in micro-fabricated capacitive sensors where the thickness of the sensor can be between 10 and 100 microns, while the lateral dimensions are of the order of 100 – 500 microns. Due to the large dielectric constant of water and tissues that surround the sensor during in vivo applications, the magnitude of the stray capacitance can be relatively large (10s or even 100s of pico Farads, pF) compared to the range of measurement of the sensor (0.1-10 pF).

From equation (13), any two electronic components in a circuit with different potentials will also create capacitance, in addition to the capacitance between the sensor's electrodes, and that is called parasitic capacitance. All the electrodes, traces, leads and solder pads on the circuit board with different potentials contribute to parasitic capacitance. The equivalent circuit of a capacitive pressure sensor will therefore consist of three capacitors in parallel, as shown in Figure 47b, where one capacitance is due to the applied pressure, a second capacitance is stray capacitance due to surrounding materials and a third one is due to internal electric fields between the measurement components on the circuit board.

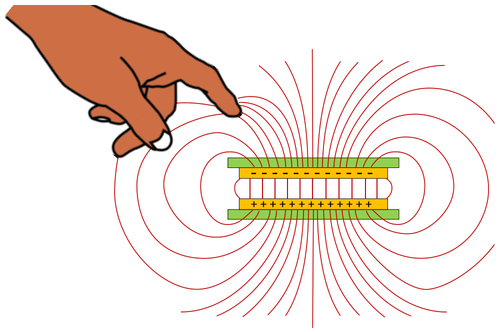

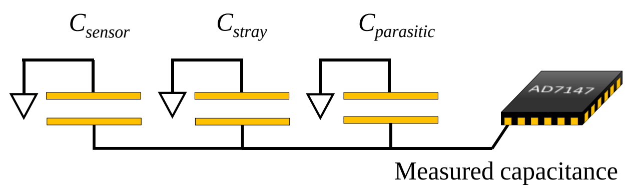

Figure 47: a) Fringe electric field bending toward human tissue that is in close proximity to capacitive sensors, b) Equivalent circuit of a pressure sensor with stray and parasitic capacitances.

The total measured capacitance value in Figure 47b will be

$$C_{total} = C_{sensor} + C_{stray} + C_{parasitic} \tag{15}$$

where the only real capacitance of interest is C_{sensor}.

To measure sensor capacitance in real time, a capacitance to digital converter (CDC) chip such as the Analog Devices AD7147 is often utilized. This 16 bit 4×4 mm^2 chip can be connected simultaneously to 12 capacitors and can measure a capacitance change of up to ±8 pF relative to ground in real time. The capacitance is measured by sending a 250 kHz square wave signal to charge and discharge the capacitors and measuring the time constant for the same.

In order to eliminate stray capacitance for in vivo applications, this thesis proposes that the sensor be covered by an active Faraday cage [53], [54], as shown in Figure 48b. The Faraday cage consists of a highly conductive material that surrounds the entire sensor. Figure 48a shows a schematic of the original sensor consisting of parallel plate electrodes made of copper on a polyimide substrate. The fringe electric fields outside the sensor are illustrated in Figure 48a. To eliminate stray capacitance from being measured by the CDC chip, this thesis proposes that the active square wave voltage supplied to the electrode for purposes of capacitance measurement be simultaneously supplied to the Faraday cage, as shown in Figure 48c. The Faraday cage voltage $V_{acs}(t)$ is then driven to the same voltage potential as the sensing electrode $V_s(t)$ always, to make the capacitance between the Faraday cage and the sensing electrode to be zero. Then any capacitance created by external fringe fields between the Faraday cage and neighboring materials will not affect the capacitance measurement. In the ideal case the stray capacitance can be completely reduced to zero in this case. Figure 48b shows the fringe electric fields being confined entirely to stay within the Faraday cage.

Note that while the use of a Faraday cage to protect humans from lightning and other similar applications are well known, the use of a transparent thin Faraday cage which is supplied an active capacitive sensing voltage to shield a micro-sensor from stray capacitance is a novel technique that is being proposed for the first time in this thesis.

For fabricating the Faraday cage gold is chosen as a highly conductive material (resistivity = $2.44\times10^{-8}\ \Omega.m$). The nominal resistance of the Faraday cage layer can be calculated using equation (16)

$$R = \rho.\frac{l}{A} \tag{16}$$

ρ is the gold resistivity and is 2.44×10^{-8} $\Omega.m$. The length of the Faraday cage is 6 cm, its thickness is 400 nm and its effective width is about 1 mm. Plugging these parameters in equation 16 gives the resistance R = 3.5 Ω.

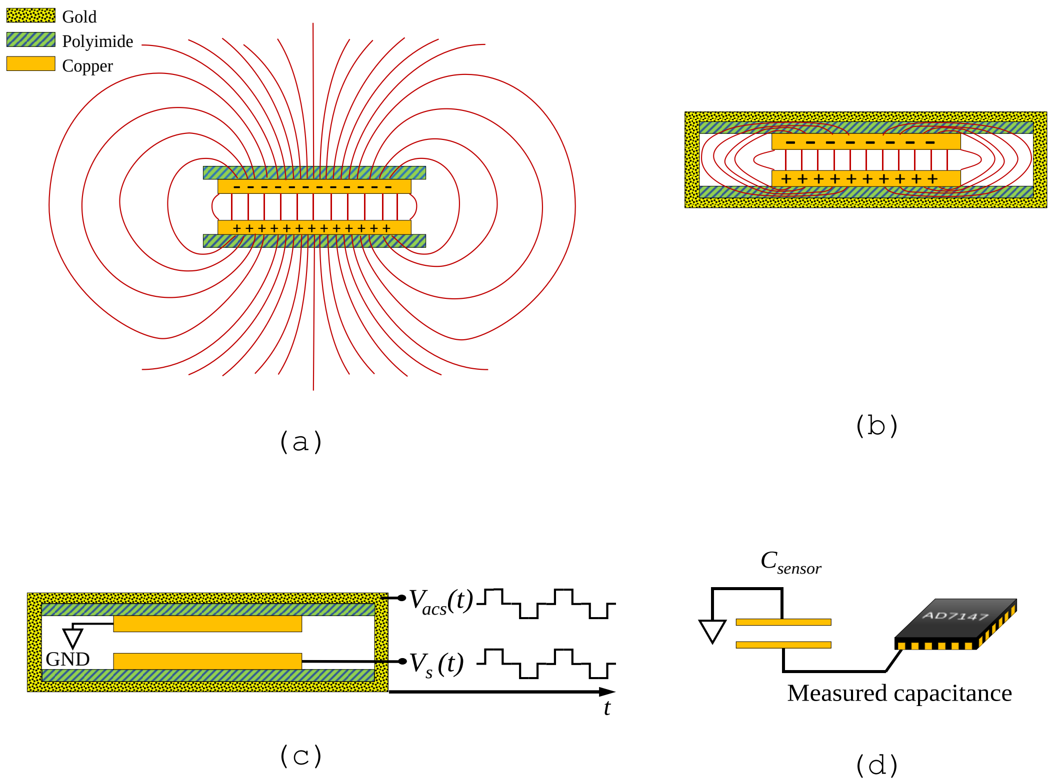

Figure 48: a) Fringe electric field in a capacitor without a Faraday cage, b) Electric field is separated from the outside world by adding a Faraday cage, c) Faraday cage is actively driven to have the same potential as the sensing electrode, d) Equivalent circuit of a shielded capacitive sensor with a Faraday cage.

4.2 Results with Active Faraday Cage

Two assembled sensors, one with an active Faraday cage on it and the other one without a Faraday cage, were tested in DI water. The results for all individual sensors of each of the sensing strips are shown in Figure 49a and Figure 49b. In Figure 49a, region 1 consists of the time when the sensor is dry and outside DI water, region 2 consists of the time when the sensor is immersed in water and region 3 consists of the time when the sensor has been removed from water but is still wet with residual water. The residual water creates stray capacitance in region 3 since the water dries up slowly. The immersion in water and subsequent removal are repeated several more times. Region 4 represents the last time that the sensor is pulled out of the water. It can be seen in Figure 49a that when the sensing strip is not shielded by the Faraday cage, the values of the stray capacitance due to the water range from 25 fF to 375 fF (femto Farad).

Then the same test is repeated in DI water with a sensing strip covered by an active Faraday cage, as shown in Figure 49b. Again, in region 1 the sensor is outside DI water and the readout is zero. Then the strip is immersed in DI water (region 2) and taken out (region 3). It can be seen in Figure 49b that the stray capacitance has dropped dramatically by factor of ~ 10 compared to Figure 49a for the sensor without the Faraday cage. It ranges from only 5fF to 42 fF. Again, there is an offset in region 3 relative to region 1. It is because after removing the sensor from water, it is still covered by a layer of water that creates stray capacitance which would gradually go to zero after drying for a long time.

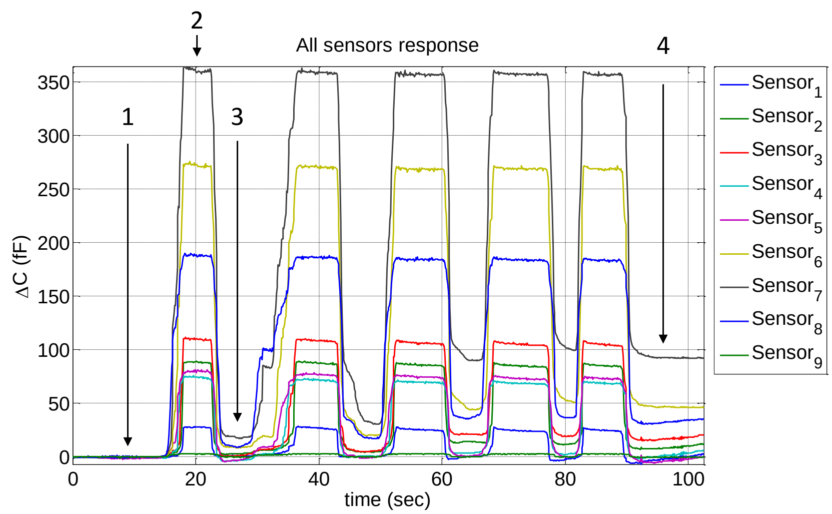

(a)

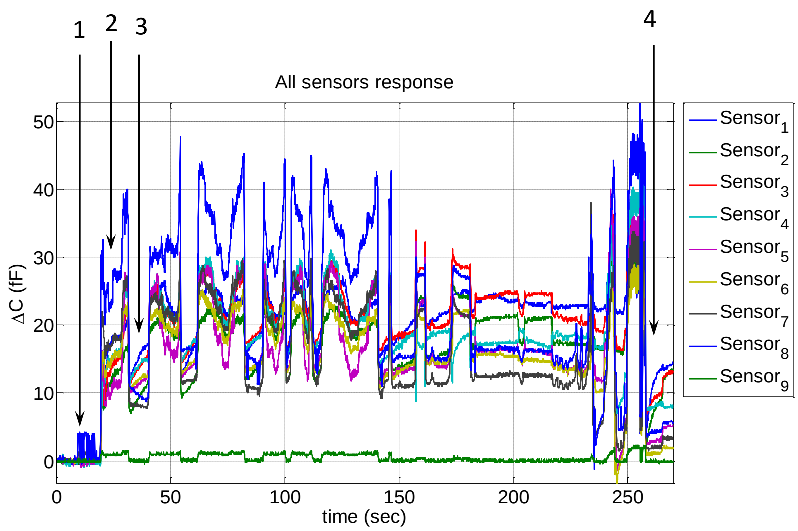

(b)

Figure 49: a) Tests of the sensor without an active Faraday cage in DI water, b) Tests of the sensor with active Faraday cage in DI water.

From Figure 49a and Figure 49b, it can be concluded that the addition of the active Faraday cage highly reduced the stray capacitance, but did not eliminate it. The reasons for the stray capacitance not being completely eliminated include:

1- The low thickness of the golden enclosure (400 nano-meters) which limits its conductivity.

2- The numerous holes that are etched to make the Faraday cage transparent, reduces material from this shielding layer and so reduces the conductivity of the Faraday cage which leads to lower functionality of the Faraday cage.
3- The lack of a Faraday cage on the sides of the sensor, since the Faraday cage is deposited on the top and bottom electrodes only.
4- The inability of the AD7147 chip to provide adequate current to completely maintain the same voltage on the Faraday cage and on the positive electrodes, even when the Faraday cage is loaded by tissues and water.

Although the stray capacitance could not be completely eliminated, it is indeed reduced approximately by a factor of 10 by the developed active Faraday cage technique.

Chapter 5

5 IN VIVO TESTS

5.1 Female Live Dog

The first tests were done on a female hound dog (Figure 50). During the tests we found out that the passage to the urethra is too long in the dog and the sensing strip cannot reach the urethra. Hence in vivo experimental data could not be obtained on the dog. A search for a better animal model to implement the tests began which led to the female sheep model that is explained in the next section.

Figure 50: Female hound dog in urodynamics test

5.2 Female Live Sheep as the Model

After calibration and in-vitro tests of the pressure sensing catheter in the extracted urethra that is discussed in chapter 4, a female sheep is selected as the suitable model for doing live in-vivo tests for two reasons: first, the urethral length in adult female sheep is about 4 cm long which is about the same size as in a human being (Figure 51) and second, catheters up to a 16 Fr Foley catheter size can be inserted in the female sheep urethra.

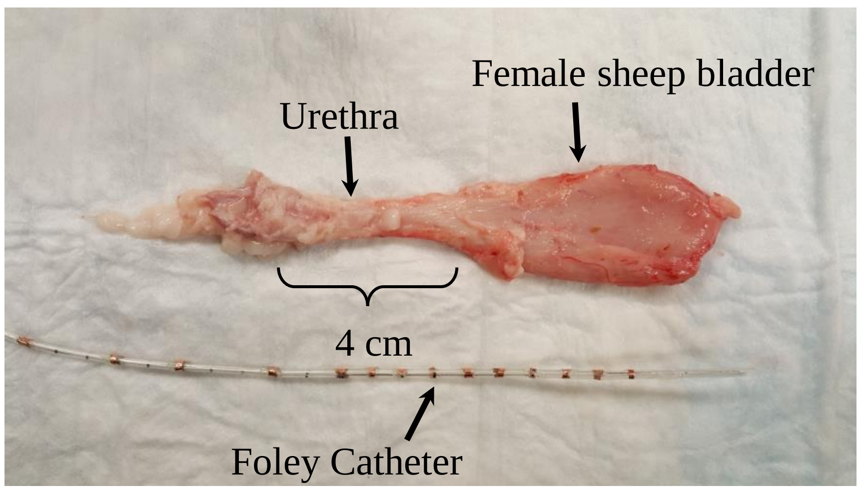

Figure 51: Extracted bladder and urethra of female sheep.

The iv-vivo tests were done in Experimental Surgical Services (ESS) at the University of Minnesota on a 98 kg female sheep (IACUC 1507-32815A). The sheep is anesthetized during the pressure measurement test. An x-ray system is available to use after the catheterization in order to find the location of the sensors in the urethra (Figure 52). During the test two technicians were monitoring the status of the sheep while one person is catheterizing it.

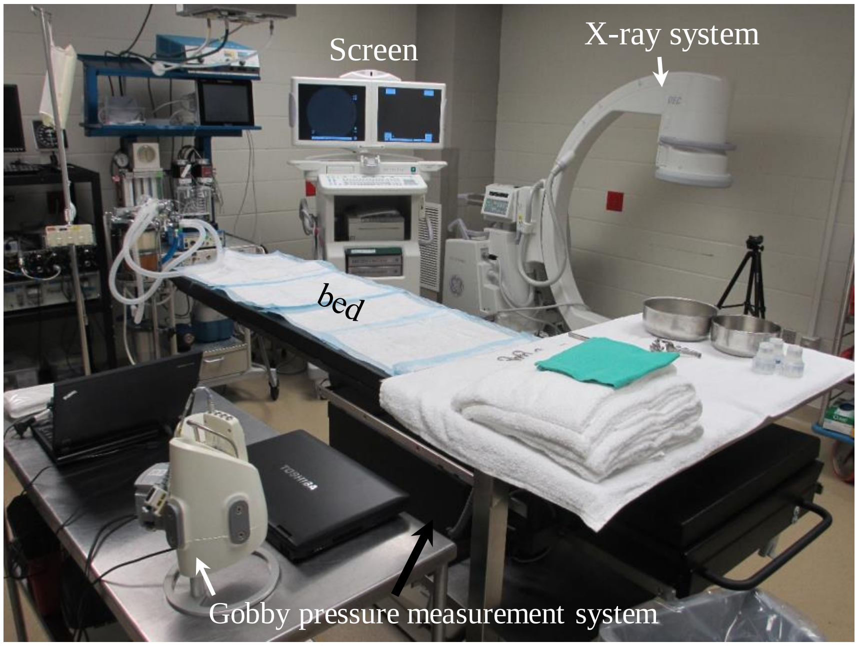

Figure 52: ESS room to test the sensing catheter.

The sheep was anesthetized during the (Figure 53). We did two sets of experiments on the sheep. In the first one we used a Goby™ portable urodynamics balloon system and inserted a 7 Fr Foley catheter to find the urethral pressure profile and in the second experiment we used our fabricated sensing catheter and recorded the pressure profile.

Figure 53: UPP test on 98 kg female sheep.

5.3 Constructing Urethral Pressure Profile Using T-DOC Catheter

In the first test, we used a T-DOC catheter and a Goby™ portable urodynamics system to measure pressure profile in the female sheep's urethra. A 7 Fr T-DOC catheter was connected to the external pressure transducer and the balloon sensor was partially charged as is mentioned in the manual. This balloon is connected through two narrow lumens to a pressure transducer outside. This transducer is connected to the software by wireless connection. The resolution of this setup is 1 cmH_2O.

We inserted the 7 Fr catheter for about 7 cm to make sure that the balloon has passed the 4 cm length of the urethra and reached the bladder (Figure 54).

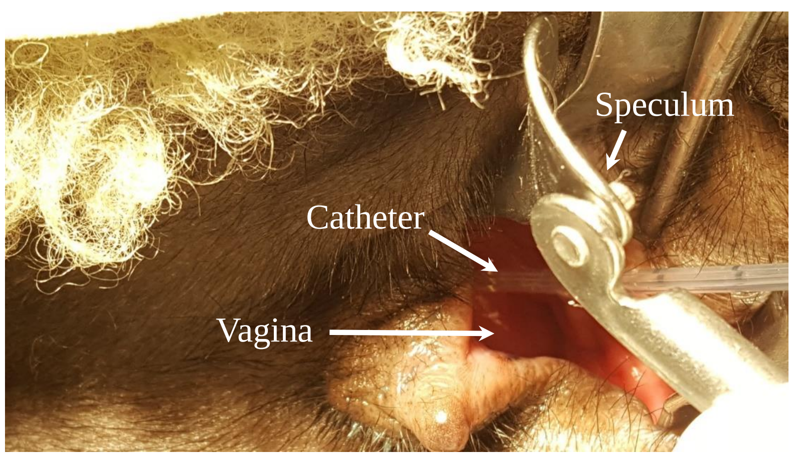

Figure 54: A 7 Fr T-DOC catheter is inserted in the urethra.

After the balloon sensor was inserted inside the bladder, we started to pull out the catheter slowly and record pressure magnitude at every 1 cm to find the UPP. The variability of the measured value was more than we expected and was about 10 cmH_2O. Because the sensor is a partially inflated balloon (chapter 4) the measured pressure value is the average value integrated on the perimeter of the urethra. Also, we observed that the pulling speed affects the pressure value and thus we would stop at every 1 cm for 5 sec and record the pressure value. The pressure profile is constructed then and is shown in Figure 55.

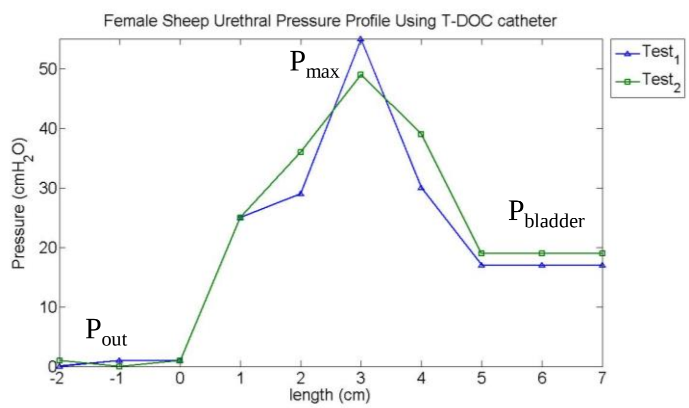

Figure 55: UPP constructed by pulling the T-DOC catheter

As it can be seen in Figure 55 the pressure in the bladder is about 20 cmH_2O and becomes maximum in the middle of the urethra (~55 cmH_2O) . Then the pressure drops to 0 cmH_2O as the balloon sensor comes out of the urethra.

5.4 Recording UPP Using the Capacitive Sensing Catheter

In the second experiment, we used the new fabricated sensing catheter to construct the real time UPP while the sheep was under anesthetization. The data acquisition started when the catheter was outside the urethra. Then the catheter was inserted and left inside the urethra for about 30 sec. during this time period pressure profile was recorded along the urethra (Figure 56). Then the catheter was pulled out slowly.

The recording was stopped after 15 sec. The sampling rate of the CDC chip is about 11 Hz (11 samples of all sensors in a second).

Figure 56: Capacitive pressure sensing catheter inserted in the sheep urethra.

5.5 Data and Discussion

The recorded pressure vs location of the sensors of the sensing strip is shown in Figure 57. During the test, sensors 1 to 4 are outside the urethra and hence are not under pressure, while sensors 5 to 9 are inside the urethra. The distance between two successive sensors is 5 mm. The maximum pressure was measured at the center of the urethra 2 cm far from the urethral opening. The magnitude is 85 cmH_2O. The measured value is 20 cmH_2O off compared to the maximum recorded pressure magnitude by the T-DOC catheter. It can be because of two sources of errors: one, the capacitive sensor measures the pressure value at one point unlike the T-DOC balloon sensor that measures the average value of pressure inside the urethra and two, as it is seen in Figure 59 the sensing strip is bent inside the urethra due to loads from the tissue and the wires and connections outside the urethra. Bending causes compression and tension in different layers of the catheter that creates strain and change between the distances of different layers. This change causes the distance of the two electrodes to change which results in capacitance change.

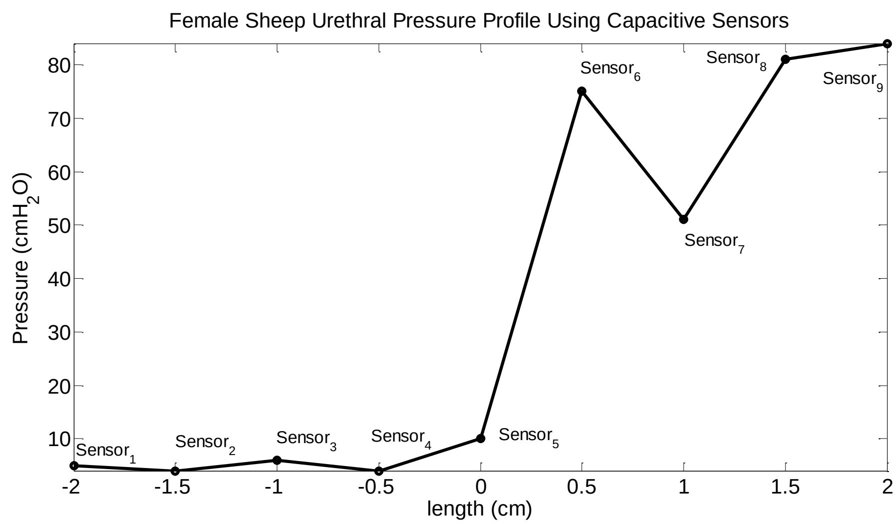

Figure 57: UPP constructed in real-time by the capacitive pressure sensing strip.

After recording pressure profile in the urethra, the sensing catheter was removed slowly from the urethra. Pressure change for every single sensor during removal from the urethra is shown in Figure 58.

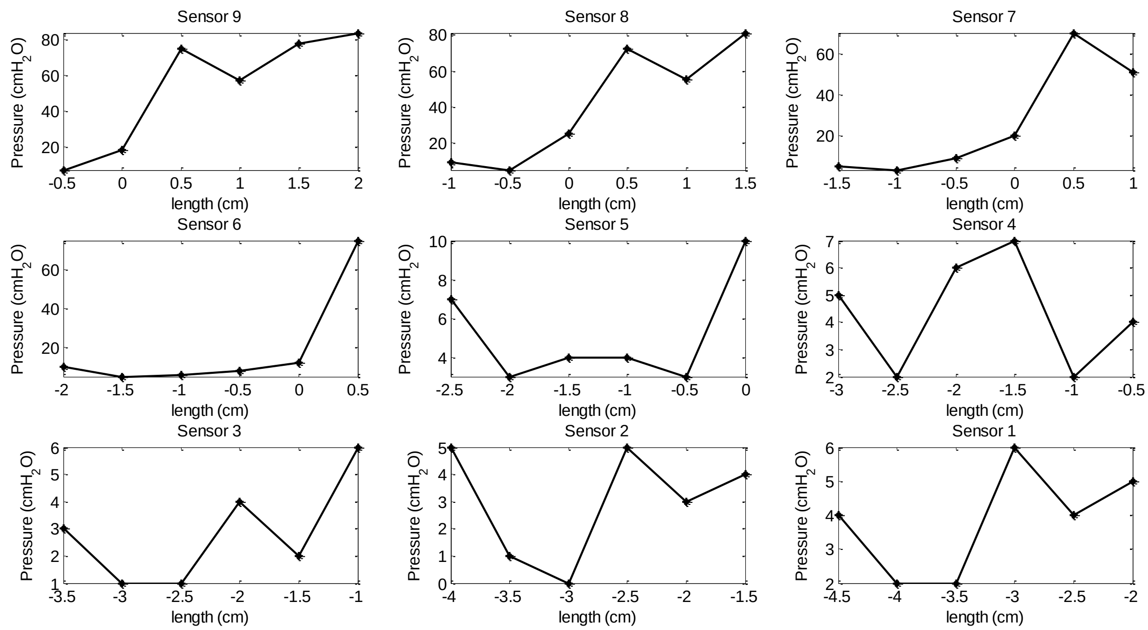

Figure 58: pressure values as the catheter is pulled out the urethra.

5.6 Summary of the Animal Tests

The sensing catheter was tested inside a female sheep's urethra. The Goby™ portable urodynamics system and a 7 Fr T-DOC (T-DOC7FS) catheter was first used to construct the reference pressure profile inside the urethra. Then the new sensing catheter was tested. The stray capacitance was significantly decreased by having the Faraday cage. The remaining stray capacitance was compensated using the reference electrodes. The measured maximum pressure value is 20 cmH_2O larger than the value from the UPP constructed by T-DOC catheter. It is expected to be because of the bending and twisting in the catheter. During a test using the x-ray system we were able to locate the sensing catheter in the urethra (Figure 59). It can be seen in Figure 59 that the catheter is bent and slightly twisted in the urethra.

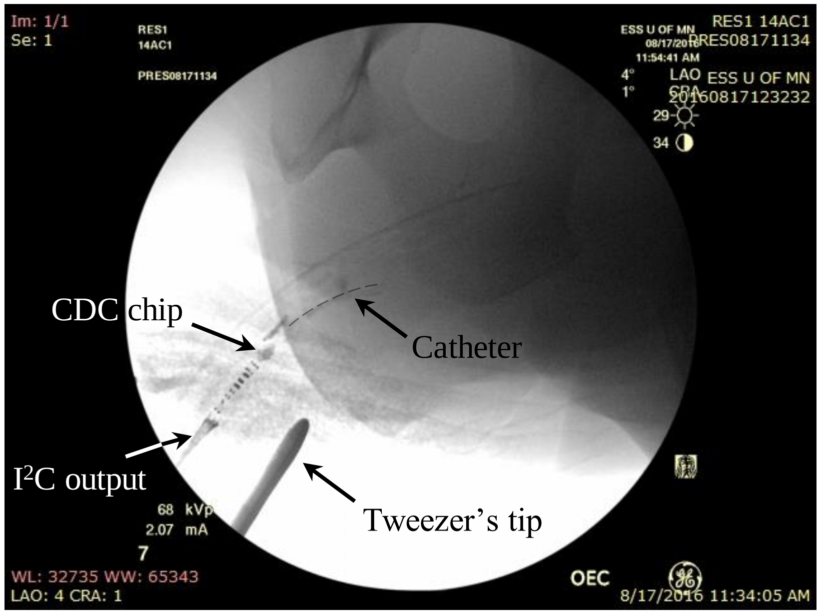

Figure 59: X-ray image of the sensing catheter after insertion in the urethra.

To decrease the effect of bending, the sensing element's design can be modified. Instead of having rectangular electrodes along the catheter having them perpendicular to it and wrapped around the catheter would reduce the effect of bending.

Chapter 6

6 CONCLUSIONS

This thesis proposed a new solution to make an inexpensive, disposable sensing strip that can be installed on Foley catheters of various sizes. A flexible capacitive sensor strip was micro fabricated and calibrated first with high sensitivity using an air pressure chamber. It's robustness in a liquid environment was verified. This instrumented catheter gives instantaneous real time pressure at 9 points in the urethra and constructs the UPP instantaneously. This addresses the old problem of having to move the catheter slowly through the patient's urethra to construct the UPP and avoids otherwise common tubing complexities in the pressure measurement. Its sampling rate allows it to even obtain the UPP during fast maneuvers such as coughing. The performance of the sensing catheter was studied in an ex-vivo human-like urethral setup developed in the lab using an extracted sheep bladder and urethra. Two cuffs on the urethra and variable pressure in the cuffs were used to create distributed pressure profiles.

A golden, thin, transparent flexible Faraday cage was micro-fabricated on the outer layer of the flexible pressure sensing strip to shield the capacitors from stray capacitance. The shielding is achieved by supplying the voltage from the capacitance sensing chip simultaneously to both the positive sensor electrode and the Faraday cage. Transparency is achieved by patterning the gold cage to create a see-through mesh. The transparency enables the top, middle and bottom layers of the sensors to be aligned accurately and then assembled together. The performance of the active Faraday cage was evaluated by testing the sensors through immersion in DI water and comparing the results with those from the sensor without a Faraday cage. It was shown that adding the Faraday cage decreases the stray capacitance by one order of magnitude. The developed active Faraday cage technique will be useful for many types of capacitive micro-sensors during in vivo measurements.

To fully remove the stray influence of urethral tissues, a reference fringe capacitance measurement sensor was also incorporated on the strip that responded only to stray capacitance. Then the stray capacitance due to tissue was removed using a compensation algorithm. The results were quantitatively verified with repeated measurements using a Goby™ portable urodynamics system.

The new catheter was tested in vivo on live sheep using an IACUC approved protocol. The instrumented catheter was able to measure pressure distribution in the urethra and provided values of the same order of magnitude as the T-DOC catheter.

The instrumented catheter got significantly bent during the live sheep tests during insertion into the urethra. Strategies for sensor re-design to avoid errors due to bending were discussed in the thesis.

REFERENCES

[1] Abrams, P; et al., "The standardization of terminology of lower urinary tract function recommended by the international continence society," *International Urogynecology Journal,* vol. 1, no. 1, pp. 45-58, 1990.

[2] Schulman, C; Claesm, H; Mattijs, J, "Urinary incontinence in Belgium: a population based epidemiological," *Euro Urol.,* vol. 32, p. 315, 1997.

[3] Herzog, AR; Fultz, NH, "Prevalence and incidence of urinary incontinence in community-," *J. Am. Geriat. Soc.,* vol. 38, p. 273, 1990.

[4] Damian, J; Martin-Moreno, JM; Lobo, F; Bonache, J; Cervino, J;, "Prevalence of urinary incontinence among Spanish older people living at home," *Eur. Urol.,* vol. 34, p. 333, 1998.

[5] Diokno, AC; Brock, BM; Brown, MB; Herzog, R, "Prevalence of urinary incontinence and other urological symptoms in the noninstitutionalized elderly," *J. Urol.,* no. 132, p. 1022, 1986.

[6] Ueda, T; Tamaki, M; Kageyama, S; Yoshimura, N; Yoshida, O, "Urinary incontinence among community-dwelling people aged 40 years or older in Japan: prevalence, risk factors, knowledge and self perception," *Int. J. Urol.,* vol. 7, p. 95, 2000.

[7] Wagner, TH; Hu, TW, "Economic costs of urinary incontinence in 1995," *Urology,* vol. 3, no. 51, pp. 355-361, 1998.

[8] Fenely, RC; Sheperd, AM; Powell, PH; Blannin, J, "Urinary incontinence: prevalence and needs," *Br. J. Urol.,* vol. 493, no. 51, 1979.

[9] Yarnell, JWG; Leger, AS, "The prevalence, severity and factors associated with urinary incontinence in a random sample of the elderly," *Age, Ageing,,* no. 8, p. 81, 1979.

[10] Abrams, P, Urodynamics, London: Springer-Verlag, 1997.

[11] Schafer, W; et al., "Good urodynamic practices: uroflowmetry, filling cystometry, and pressure-flow studies," *Neurourol Urodyn,* vol. 3, no. 21, pp. 261-74, 2002.

[12] Griffiths, C.J.; et al., "Ambulatory monitoring of bladder and detrusor pressure during natural filling," *J Urol* , vol. 3, no. 142, pp. 780-784, 1989.

[13] Webb, R.J; Ramsden, P.D; Neal, D.E, "Ambulatory monitoring and electronic measurement of urinary leakage in the diagnosis of detrusor instability and incontinence," *J Urol,* vol. 2, no. 68, pp. 148-152, 1991.
.

[14] Resplande, J; et al., "Urodynamic changes induced by the intravaginal electrode during pelvic floor electrical

stimulation.," *Neurourol Urodyn,* vol. 1, no. 22, pp. 24-28, 2003.

[15] Lapides, J; Ajemian, EP; Stewart, BH; Breakey BA; Lichtwardt, JR, "Further observations on the kinetics of the urethrovesical sphincter," *J. Urol.,* pp. 84-96, 1960.

[16] Brown, M; Wickham, J.E.A;, "The urethral pressure profile," *British Journal of Urology,* no. 41, p. 211, 1969.

[17] Jonas, U; Tanagho, E.A, "Urethral profile measurement with modified Enhorning catheter," in *Continence Society Conference*, Glascow, 1975.

[18] Cooper, MA; Fletter, PC; Zaszczurynski, PJ; et al., "Comparison of air-charged and water-filled urodynamic pressure measurement catheters," *Neurourol Urodyn,* no. 30, p. 329–34, 2011.

[19] "Luna Micro-tip Catheters for Urology Measurement," [Online]. Available: http://www.mmsinternational.com/int/761/urology-ambulatory-urodynamics-product-luna-catheters. [Accessed 18 5 2017].

[20] Ahmadi, Mahdi; Rajamani, Rajesh; Timm, Gerald; Sezen, Serdar, "Flexible Distributed Pressure Sensing Strip for a Urethral Catheter," *Journal of Microelectromechanical Systems,* vol. 24, no. 6, 2015.

[21] Yao, J; Li D , "Research on a Novel Magnetic Fluid Micro-Pressure Sensor," *Measurement Science and Technology,* vol. 26, no. 7, 2015.

[22] Cheng, R; Li, C; Zhao, Y; Li, B; Tian, B, "A High Performance Micro-Pressure Sensor Based on a Double-Ended Quartz Tuning Fork and Silicon Diaphragm in Atmospheric Packaging," *Measurement Science and Technology,* vol. 26, no. 6, 2015.

[23] Takahashi, H; Matsumoto, K; Shimoyama, I, "Differential Pressure Distribution Measurement for the Development of Insect-Sized Wings," *Measurement Science and Technology,* vol. 24, no. 5, 2013.

[24] Eaton, W. P; Smith, J. H, "Micromachined pressure sensors: review and recent developments," *Smart Materials and Structures,* vol. 6, no. 5, 1999.

[25] Aguilera-Servin, J; Miao, T.; Bockrath, M., "Nanoscale pressure sensors realized from suspended graphene membrane devices," *Applied Physics Letters,* vol. 106, no. 083103, 2015.

[26] Mastronardi, V. M., Ceseracciu, L; Guido, F; Rizzi, F.; Athanassiou, A.;De Vittorio, M.; Petroni, S., "Low stiffness tactile transducers based on AlN thin film and polyimide," *Applied Physics Letters,* vol. 106, no. 162901, 2015.

[27] Lu, Y; Cottone, F; Boisseau, S; Marty, F; Galayko, D; Basset,P, "A nonlinear MEMS electrostatic kinetic energy

harvester for human-powered biomedical devices," *Applied Physics Letters,* vol. 107, no. 253902, 2015.

[28] Li, B; Fontecchio, A. K; Visell, Y, "Mutual capacitance of liquid conductors in deformable tactile sensing arrays," *Applied Physics Letters,* vol. 108, no. 013502, 2016.

[29] Liu, H; Pike, W. T. , "A micromachined angular-acceleration sensor for geophysical applications," *Applied Physics Letters,* vol. 109, no. 173506, 2016.

[30] Ponnamma, D; Sadasivuni, K. K; Cabibihan, J.J; Yoon W. J; Kumar, B. , "Reduced graphene oxide filled poly(dimethyl siloxane) based transparent stretchable, and touch-responsive sensors," *Applied Physics Letters,* vol. 108, no. 171906, 2016.

[31] Yu, F. L; Kim, B. J; Meng, E, "Chronically Implanted Pressure Sensors: Challenges and State of the Field," *Sensors,* 2014.

[32] Mannsfeld, S. C. B; Tee, B. C.-K; Stoltenberg, R. M; Chen, H; Barman, S; Muir, B. V. O; Sokolov, A. N. R. C; Bao, Z, "Highly sensitive flexible pressure sensors with microstructured rubber dielectric layers," *Nature materials,* 2010.

[33] Zhu, S.E; Ghatkesar, M. K; Zhang, C; Janssen, M. , "Graphene based piezoresistive pressure sensor," *APPLIED PHYSICS LETTERS,* 2013.

[34] Tadigadapa, S.; Mateti, K, "Piezoelectric MEMS Sensors: State-of-the-art and perspectives," *Measurement Science and Technology,* vol. 20, no. 9, 2009.

[35] Dagdeviren, C.; Ozlem, P. J; Tuzman, L; Park, K; Lee, K. J; Shi, Y.;Huang, Y; Rogers, J. A, "Recent progress in flexible and stretchable piezoelectric devices for mechanical energy harvesting, sensing and actuation," *Extreme mechanics letters,* vol. 9, no. 1, pp. 269-281, 2016.

[36] Kim, S.C.; Wise, K.D., "Temperature Sensitivity in Silicon Piezoresistive Transdcuers," *IEEE Transactions on Electron Devices,* vol. 30, no. 7, pp. 802-810, 1983.

[37] Ahmadi, M; Rajamani, R; Timm, G; Sezen, S, "Instrumented Urethral Catheter and Its Ex-Vivo Validation in a Sheep Urethra," *Measurement science and technology,* 2017.

[38] Sezen, A.S.; Rajamani, R; Morrow, D; Gilbert, B; Kaufman, K. R, "An Ultra-Miniature MEMS Pressure Sensor with High Sensitivity for Measurement of Intra-Muscular Pressure in Patients with Neuro-Muscular Diseases," *ASME Journal of Medical Devices,* vol. 3, no. 3, 2009.

[39] Peng, P; Rajamani, R; Erdman, A.G., "Flexible Tactile Sensor for Tissue Elasticity Measurements," *IEEE/ASME Journal of Microelectromechanical Systems,* vol. 18, no. 6, pp. 1226-1233 , 2009.

[40] Ahmadi, M. ; Rajamani, R; Timm, G.; Sezen,S, "Distributed pressure sensors for a urethral catheter,"

in *Engineering in Medicine and Biology Society (EMBC)*, 2015.

[41] Y. Zhang, R. Howver, B. Gogoi and N. Yazdi, "A high sensitive ultra-thin MEMS capacitive pressure sensor," *IEEE Transducers,* 2011.

[42] Marioll, D;Sardini, E; Taroni, A, "High accuracy measurement techniques for capacitance measurement," *Measurement Science and Technology,* 1993.

[43] Heerens, W. C. , "Application of capacitance techniques in sensor design," *Journal of Physics E: Scientific Instruments,* 1986.

[44] Puers, R., "MEMS capacitive sensor interface: can we solve the challenge?," in *Sensors+Test Conference*, 2009.

[45] R. Puers, "MEMS capacitive sensor interface: can we solve the challenge?," in *Sensors+Test Conference*, 2009.

[46] "Cardio-MEMS reference".

[47] Najafi, N; Ludomirsky, A, "Initial Animal Studies of a Wireless Battery-Less MEMS Implant for Cardiovascular Applications," *Biomedical Microdevices,* vol. 6, no. 1, pp. 61-65, 2004.

[48] Chen, P.J.; Rodger, D.C; Agrawal, R; Saati, S; Meng, E; Varma, R; Humayun,M.S.; Tai, Y.C, "Implantable Micromechanical Parylene-Based Pressure Sensors for Unpowered Intraocular Pressure Sensing," *Journal of*

Micromechanics and Microengineering, vol. 17, no. 10, pp. 1931-1938, 2007.

[49] Yoon, H.J; Jung, J.M; Jeong, J.S; Yang, S.S. , "Micro Devices for a Cerebrospinal Fluid Shunt System," *Sensors and Actuators A:Physical,* vol. 110, no. 1, pp. 68-76, 2004.

[50] Harrison, N. W, "REVIEW : The Urethral Pressure Profile, St. Peter's Hospitals and Institute of Urology," *Urological Research,* vol. 4, pp. 95-100, 1976.

[51] Senturia, S.D., Microsystem Design, New York: Springer, 2004.

[52] Giovanni, M. D, Flat and Corrugated Diaphragm Design Handbook, New York: Marcel Dekker, 1982.

[53] Chapman, S. J; Hawett, D. L. P; Trefethen, N, "Mathematics of the Faraday Cage," *SIAM Review,* vol. 57, no. 3, pp. 398-417, 2015.

[54] Huangt, S. M; Stottf, A. L; Greenf, R. G; Beck, M. S, "Electronic transducers for industrial measurement of low value capacitance," *Journal of Physics E: Scientific Instruments,* 1988.